Processes controlling the seasonal variations of ^{210}Pb and ^{7}Be at the Mt. Cimone WMO-GAW global station, Italy: A model analysis

Erika Brattich[1], Hongyu Liu[2], Laura Tositti[1], David B. Considine[3], and James H. Crawford[4]

[1] Department of Chemistry "G Ciamician", Alma Mater Studiorum University of Bologna, Bologna (BO), 40126, Italy

[2] National Institute of Aerospace, Hampton, Virginia, Virginia, VA 23681, USA

[3] NASA Headquarters, Washington, DC 20546, USA

[4] NASA Langley Research Center, Hampton, Virginia, VA 23681, USA

Correspondence to: Hongyu Liu (hongyu.liu-1@nasa.gov)

Abstract. We apply the Global Modeling Initiative (GMI) chemistry and transport model driven by the NASA's MERRA assimilated meteorological data to simulate the seasonal variations of two radionuclide aerosol tracers (terrigenous ^{210}Pb and cosmogenic ^{7}Be) at the WMO-GAW station of Mt. Cimone (44°12' N, 10°42' E, 2165 m asl, Italy), which is representative of free-tropospheric conditions most of the year, during 2005 with an aim to understand the roles of transport and precipitation scavenging processes in controlling their seasonality. The total precipitation field in the MERRA data set is evaluated with the Global Precipitation Climatology project (GPCP) observations, and a generally good agreement is found. The model reproduces reasonably the observed seasonal pattern of ^{210}Pb concentrations, characterized by a wintertime minimum due to lower ^{222}Rn emissions and weaker uplift from the boundary layer and summertime maxima resulting from strong convection over the

continent. The observed seasonal behavior of ^{7}Be concentrations shows a winter minimum, a summer maximum, and a secondary spring maximum. The model captures the observed ^{7}Be pattern in winter-spring, which is linked to the larger stratospheric influence during spring. However, the model tends to underestimate the observed ^{7}Be concentrations in summer, partially due to the sensitivity to spatial sampling in the model. Model sensitivity experiments indicate a dominant role of precipitation scavenging (versus dry deposition and convection) in controlling the seasonality of ^{210}Pb and ^{7}Be concentrations at Mt. Cimone.

1 Introduction

The use of atmospheric radionuclides to understand atmospheric dynamics, pollution transport and removal processes has a long history (e.g., Junge, 1963; Reiter et al., 1971; Gäggeler, 1995; Arimoto et al., 1999; Turekian and Graustein, 2003; WMO-GAW, 2004; Dibb, 2007; Rastogi and Sarin, 2008; Froehlich and Masarik, 2010; Lozano et al., 2012). It has been recognized that natural radionuclides are useful in a global monitoring network for atmospheric composition to support global climate change and air quality research, and therefore they are measured at many of the regional, global and contributing-partner stations in the Global Atmosphere Watch (GAW) network of the World Meteorological Organization (WMO) (WMO-GAW, 2004). In particular, terrigenous ^{210}Pb and cosmogenic ^{7}Be natural radionuclides are helpful in the understanding of the roles of transport and/or scavenging in controlling the behaviors of radiatively active trace gases and aerosols (Feichter et al., 1991; Balkanski et al., 1993; Koch et al., 1996), as well as their anthropogenic (vs. natural) origin (e.g., Graustein and Turekian, 1996; Arimoto et al., 1999; Liu et al., 2004; Cuevas et al., 2013). They are routinely monitored at WMO-GAW stations around the world (Lee et al., 2004). Although ^{210}Pb and ^{7}Be have long (1998-2011) been measured at the Global WMO-GAW station of Mt. Cimone (Italy), their seasonal behavior has not been thoroughly elucidated (Lee et al., 2007; Tositti et al.,

2014). Here we apply a state-of-the-art global chemistry and transport model (CTM) to the simulation of ^{210}Pb and ^{7}Be, with an objective to better understand the roles of transport and precipitation scavenging processes in controlling their seasonal variations at Mt. Cimone.

Because of their contrasting natural origins, ^{210}Pb and ^{7}Be have been used as a pair to study the vertical transport and scavenging of aerosols (Koch et al., 1996). ^{210}Pb (half-life $\tau_{1/2}$ = 22.3 years) is the decay daughter of ^{222}Rn ($\tau_{1/2}$ = 3.8 days), which is emitted from soils by decay of ^{226}Ra. The oceanic input of ^{222}Rn is about two orders of magnitude less than the continental input and, because of the continental origin of ^{222}Rn, ^{210}Pb is considered as a tracer of air masses with continental origin (Baskaran, 2011). ^{7}Be ($\tau_{1/2}$ = 53.3 days) is a cosmogenic radionuclide generated by cosmic ray spallation reactions with nitrogen and oxygen (Lal et al., 1958). Most (~67%) of ^{7}Be is produced in the stratosphere and the remaining (~33%) is generated in the troposphere, particularly in the upper troposphere (Johnson and Viezee, 1981; Usoskin and Kovaltsov, 2008). ^{7}Be is thus considered a tracer of stratospheric influence (Viezee and Singh, 1980; Dibb et al., 1992, 1994; Liu et al., 2004, 2016) and subsidence (Feely et al., 1989; Koch et al., 1996; Liu et al., 2004). Once produced, both radionuclides rapidly attach to ubiquitous submicron aerosol particles in the ambient air (Papastefanou and Ioannidou, 1995; Winkler et al., 1998; Gaffney et al., 2004; Ioannidou et al., 2005), and are removed from the atmosphere mainly by wet and secondarily dry deposition (Kulan et al., 2006). The concentrations of these radionuclides in surface air thus depend on their sources, transport, wet and dry removal, and radioactive decay (in the case of ^{7}Be). Rainfall scavenging processes are generally more effective on ^{210}Pb than on ^{7}Be concentrations (Koch et al., 1996; Caillet et al., 2001; Likuku, 2006; Dueñas et al., 2009; Lozano et al., 2012).

Observational studies have previously been conducted to examine the factors influencing surface ^{210}Pb and ^{7}Be concentrations in Europe, the Middle East and North Africa. Different

synoptic and mesoscale patterns are associated with the ranges of ^{210}Pb and ^{7}Be activity concentrations (Lozano et al., 2012, 2013). In southwestern Spain (El Arenosillo), for instance, low ^{210}Pb values are strongly linked to air masses from the Atlantic Ocean, whereas the highest values are associated with air masses clearly under the influence of continents, such as the Iberian Peninsula and North of Africa (Lozano et al., 2012). As for ^{7}Be, the highest ^{7}Be activity concentrations over southwestern Iberian Peninsula are related with the arrival of air masses from middle latitudes, and in particular from the Canary Islands, western Mediterranean Basin and the north of Africa (Dueñas et al., 2011; Lozano et al., 2012).

With respect to ^{210}Pb and ^{7}Be spatial variability, ^{210}Pb concentrations in surface air are strongly dependent on whether it is located over land or ocean, whereas ^{7}Be concentration is mainly latitudinally dependent, due to their different production mechanisms. Generally speaking, in the Northern Hemisphere higher ^{7}Be concentrations are present at middle latitudes (20-50° N), because of the mixing of stratospheric air into the upper troposphere along the tropopause discontinuity in mid-latitude regions and subsequent convective mixing within the troposphere, which brings ^{7}Be-rich air masses into the planetary boundary layer and to the earth's surface (Kulan et al., 2006). Lower ^{7}Be concentrations are towards the pole and towards the equator (Kulan et al., 2006; Steinmann et al., 2013).

Many studies examined the seasonal behavior of ^{210}Pb and ^{7}Be at European mid-latitude surface sites (e.g., Cannizzaro et al., 1999; Ioannidou et al., 2005; Daish et al., 2005; Todorovic et al., 2005; Likuku, 2006; Dueñas et al., 2009; Pham et al., 2011; Carvalho et al., 2013; Steinmann et al., 2013). High levels of ^{210}Pb during summer and low levels in winter were found, reflecting the differing rates of ^{222}Rn emanation from soil above the European land mass during winter (wet or snow covered soil) and summer (dry soil) (Hötzl and Winkler, 1987; Caillet et al., 2001; Daish et al., 2005; Ioannidou et al., 2005). At low-elevation sites, monthly

^{7}Be averages are characterized by a well-defined annual cycle with lower values during winter and higher values during summer. Generally, the increase of ^{7}Be in ground level air from March to May is ascribed to the more efficient and higher frequency stratosphere- troposphere exchange (STE), whereas the further increase of ^{7}Be during summer is due to the stronger convective mixing and higher tropopause (Ioannidou et al., 2014). The higher tropopause height is associated with anticyclonic conditions, which results in downward transport from the upper troposphere and reduced wet scavenging during these conditions (Gerasopoulos et al., 2001, 2005; Ioannidou et al., 2014). In fact, compensating subsidence associated with convective mixing enhances downward transport of ^{7}Be from the upper troposphere (rather than direct input of stratospheric air) down to the lower troposphere and ground level (Zanis et al., 1999; Gerasopoulos et al., 2001, 2005; Ioannidou et al., 2005; Likuku et al., 2006; Steinmann et al., 2013).

High-elevation sites such as Jungfraujoch (Switerland), Zugspitze (Germany), and Mt. Cimone (Italy), typically lying above the planetary boundary layer (PBL), are characterized by lower ^{210}Pb concentrations and higher ^{7}Be due to direct influences of air masses from the free troposphere (Zanis et al., 2000). The observed seasonal ^{210}Pb pattern at the high-altitude sites of Puy de Dome (1465 m asl, France) and Opme (660 m asl, France) is characterized by maximum concentrations in spring and autumn and minimum concentrations in winter. This is due to higher radon emissions during the dry season (summer) than during the wet season (winter), and lower PBL height during winter (Bourcier et al., 2011). The latter results in weaker upward transport of ^{222}Rn and ^{210}Pb at high-altitude sites. Similar to low-elevation sites, higher ^{7}Be values are observed in summer due to convection-forced exchange with the upper troposphere and to the higher tropopause height that leads to more efficient vertical transport from the upper to lower troposphere (Reiter et al., 1983; Gerasopoulos et al., 2001; Bourcier et al., 2011). At high-altitude sites a secondary maximum of ^{7}Be during cold months (December-

March) is generally observed and attributed to the increase in stratosphere-to-troposphere events during this season (e.g., James et al., 2003; Stohl et al., 2003; Trickl et al., 2010). The higher frequency of rapid subsidence in winter at Northern Hemisphere mid-latitudes can be ascribed to the intensity of baroclinic systems, which is greatest in the wintertime. In fact, well-developed tropopause folds and rapid deep intrusions are most likely to occur in the wake of intense cyclogenesis, usually limited to the wintertime storm track regions (James et al., 2003).

Numerical models have been used to analyze ^{210}Pb and ^{7}Be observations at high-elevation sites. 1-D model simulations of surface ^{7}Be showed higher concentrations at high-elevation sites (Jasiulionis and Wershofen, 2005; Simon et al., 2009), but also suggested that the diffusion of ^{7}Be was affected by the seasonal variation of meteorological conditions. Balkanski et al. (1993) examined the transport of ^{210}Pb in a global 3-D model and reported a weak decrease of ^{210}Pb concentrations between the continental mixed layer and the free troposphere: simulated concentrations at 6-km altitude were about 50% of those in the continental mixed-layer over much of the Northern Hemisphere in summer, and over large areas of the tropics year around, a result consistent with the few observations available for the free troposphere at that time (Moore et al., 1973). Rehfeld and Heimann (1995) compared the 3-D model simulated seasonal pattern of surface ^{210}Pb and ^{7}Be concentrations with the observations at several sites in both hemispheres. At Mauna Loa (19.47°N, 155.6°W, 3400 m asl, Hawaii) ^{210}Pb seasonality was characterized by high concentrations in spring and summer and lower ones in winter, as opposed to the seasonal pattern found at higher latitudes, where the ^{210}Pb maximum concentrations in winter are attributed to the advective transport of ^{210}Pb aerosols from mid-latitudes. This behavior is due to the elevation of the site, representative of the conditions of the free troposphere rather than those of the PBL. As for ^{7}Be, the comparison between the model and the observations at Rexburg (43.8°N, 111.83°W, 1483 m asl, USA) showed systematically lower model values, due to the much higher precipitation rates in the model.

Previous studies have examined surface ^{7}Be observations at Mt. Cimone with respect to the role of STE in surface ozone increases (Bonasoni et al., 1999, 2000ab; Cristofanelli et al., 2003, 2006, 2009a, 2015; Lee et al., 2007) within the framework of European projects such as VOTALP (Vertical Ozone Transport in the Alps) and STACCATO (influence of Stratosphere-Troposphere exchange in A Changing Climate on Atmospheric Transport and Oxidation capacity). These studies led to the assessment of a higher incidence of STE events during the period from October to February relative to the warm season, when thermal convection and the rising of the tropopause promote vertical mixing, which acts as a confounding factor in STE detection. Lee et al. (2007) and Tositti et al. (2014) reported the seasonal patterns and frequency distributions of ^{210}Pb and ^{7}Be measured at Mt. Cimone, and highlighted higher concentrations of both radionuclides in the summertime due to the higher mixing height and horizontal transport by regional airflows. During winter, a general increase in ^{7}Be is associated with a decrease in ^{210}Pb, due to the dominating effect of STE and subsidence in the free troposphere. At the time of this work, no model analyses of ^{210}Pb and ^{7}Be observations at the site have been conducted.

In this paper, we conduct simulations of ^{210}Pb and ^{7}Be at Mt. Cimone with a state-of- the-art global 3-D chemistry and transport model (GMI CTM) driven by assimilated meteorological fields for the year of 2005. Our objectives are a better elucidation of the seasonal variations of ^{210}Pb and ^{7}Be concentrations and an improved understanding of the roles of transport and precipitation scavenging processes in their seasonalities at Mt. Cimone.

The remainder of this paper is organized as follows. Section 2 describes the measurement site, the radioactivity measurements at Mt. Cimone, and the GMI CTM. Section 3 evaluates the model performance in reproducing the observed wind and precipitation fields. Section 4 evaluates the seasonal ^{210}Pb and ^{7}Be concentrations in the model with those observed. Section

5 examines the sources and seasonal variations in the simulated radionuclide activities, followed by summary and conclusions in section 6.

2 Data and Methods

2.1 Radionuclide Measurements at Mt. Cimone

Mt. Cimone station (44°12' N, 10°42' E, 2165 m asl) is a global WMO-GAW station managed by the Meteorological Office of the Italian Air Force, which hosts the research platform "Ottavio Vittori" of the Institute of Atmospheric and Climate Science of the National Council of Research (ISAC-CNR). The station is located on top of the highest peak of the Italian northern Apennines, with a 360° free horizon and an elevation such that the station lies above the PBL during most of the year: the Mt. Cimone measurements are considered representative of the southern Europe/Mediterranean free troposphere (Bonasoni et al., 2000a; Fischer et al., 2003; Cristofanelli et al., 2007), although during the warmer months an influence of PBL air can be detected due both to convective processes and mountain/valley breeze regimes (Fischer et al., 2003; van Dingenen et al., 2005; Tositti et al., 2013). Note in this framework that southern Europe and Mediterranean basin are considered as a hot-spot region in terms of both climate change (e.g., Forster et al., 2007) and air quality (Monks et al., 2009), as well as a major crossroad of different air mass transport processes (Li et al., 2001; Lelieveld et al., 2002; Millàn et al., 2006; Duncan et al., 2008; Tositti et al., 2013).

At Mt. Cimone station, ^{210}Pb, ^{7}Be, and aerosol mass load in the form of PM_{10} have been regularly measured in the period of 1998-2011 with a Thermo-Environmental PM_{10} high-volume sampler. PM_{10} is sampled on rectangular glass fiber filters (Whatman, 20.3 cm × 25.4 cm, with an effective exposure area of about 407 cm^2), which were manually changed every 2-3 days, depending on weather conditions, failures of the sampling equipment and/or of the power supply and personnel on site. The average flow rate was about 1.13 m^3 min^{-1} at standard

temperature and pressure (STP), with an average volume of air collected on each filter equal to 3000-4000 m^3 (about 48 hours of sampling, 115-175 samples per year).

Airborne radionuclides travel attached to particulate matters, and as a consequence of their physical origin, tend to populate the fine fraction (<1.0 μm) (Winkler et al., 1998; Gaffney et al., 2004). The PM_{10} samples were subjected to non-destructive high-resolution γ-spectrometry for the determination of airborne radiotracers ^{210}Pb and ^{7}Be. The characteristics of the two Hyper Pure Germanium crystal detectors (HPGe) detectors are as follows: one p-type coaxial detector by Ortec/Ametek with a relative efficiency of 32.5% and FWHM 1.8 keV at 1332 keV and one planar DSG detector with an active surface of 1500 mm^2 and FWHM 0.73 keV at 122 keV, for higher and lower energy ranges (100-2000 keV and 0-900 keV), respectively.

Spectra were accumulated for at least one day to optimize peak analysis and then processed with a specific software package (GammaVision-32, version 6.07, Ortec). Efficiency calibration was determined on both detectors with a blank glass fiber filter traced with accurately weighted aliquots of a standard solution of mixed radionuclides (QCY48, Amersham) supplemented with ^{210}Pb, homogeneously dispersed dropwise over the filter surface. Once dried under a hood under ambient conditions, the calibration filter was folded into a polystyrene container in the same geometry as the unknown samples. Quantitative analysis on samples was carried out by subtracting the spectrum of a blank filter in the same geometry, while uncertainty on peaks (k = 1, 68% level of confidence) was calculated propagating the combined error over the efficiency fit previously determined with the counting error. Minimum detectable activity was calculated making use of the traditional ORTEC method (ORTEC, 2003) with a peak cut-off limit of 40%. Activity data was corrected to the midpoint of the time interval of collection and for the decay during spectrum acquisition. For our analysis, we used monthly averages of ^{210}Pb and ^{7}Be data at Mt. Cimone in 2005.

2.2 GMI Model

The Global Modeling Initiative (GMI, http://gmi.gsfc.nasa.gov) is a NASA-funded project aiming at improving assessments of anthropogenic perturbations to the Earth system; in this framework, a CTM appropriate for stratospheric assessments was developed (Rotman et al., 2001). It was firstly used to evaluate the potential effects of stratospheric aircraft on the global stratosphere (Kinnison et al., 2001) and on the Antarctic lower stratosphere (Considine et al., 2000). The recent version of the GMI CTM includes a full treatment of both stratospheric and tropospheric photochemical and physical processes and is also capable of simulating atmospheric radionuclides ^{222}Rn, ^{210}Pb, ^{7}Be, and ^{10}Be throughout the troposphere and stratosphere (Considine et al., 2004, 2005; Rodriguez et al., 2004; Liu et al., 2016). Details of the model are described in Duncan et al. (2007, 2008), Strahan et al. (2007), and Considine et al. (2008).

In this work, we simulate ^{222}Rn, ^{210}Pb, ^{7}Be, and ^{10}Be using a version of the GMI model with the same basic structure as described by Considine et al. (2005) and Liu et al. (2016), including parameterizations of the important tropospheric physical processes such as convection, wet scavenging, dry deposition and planetary boundary layer mixing. Meteorological data used to drive the CTM at 2° latitude by 2.5° longitude resolution, e.g., horizontal winds, convective mass fluxes and precipitation fields, are the Modern-Era Retrospective analysis for Research and Applications (MERRA) assimilated data set from the NASA Global Modeling and Assimilation Office (GMAO) (Rienecker et al., 2011).

The flux-form semi-Lagrangian advection scheme and a convective transport algorithm from the CONVTRAN routine in NCAR CCM3 physics package are used in the model. The wet deposition scheme is that of Liu et al. (2001): it includes scavenging in wet convective updrafts, and first-order rainout and washout from both convective anvils and large-scale precipitations. The gravitational settling effect of cloud ice particles included in Liu et al.

(2001) is not considered here. Dry deposition of aerosols is computed using the resistance-in-series approach. For the simulations of radionuclides, each simulation was run for six years, recycling the MERRA meteorological data for 2005, to equilibrate the lower stratosphere as well as the troposphere (Liu et al., 2001). The sixth-year output was used for analysis.

A uniform ^{222}Rn emission of 1.0 atom cm^{-2} s^{-1} from land under nonfreezing conditions is assumed (Liu et al., 2001). Following Jacob and Prather (1990), the flux is reduced by a factor of 3 under freezing conditions. The flux from oceans and ice is null. Although a large variability of ^{222}Rn emission from land is observed, the above emission estimate is thought to be accurate to within 25% globally (Turekian et al., 1977) and to within a factor of 2 regionally (Wilkening et al., 1975; Schery et al., 1989; Graustein and Turekian, 1990; Nazaroff, 1992; Liu et al., 2001).

Following Brost et al. (1991) and Koch et al. (1996), we used the Lal and Peters (1967) ^{7}Be source for 1958 (solar maximum year), as it best simulated stratospheric ^{7}Be concentrations measured from aircraft (Liu et al., 2001). The rates of ^{7}Be production reported more recently by Usoskin and Kovaltsov (2008) broadly agree with those of Lal and Peters (1967) with slightly (about 25%) lower global production rate and will be tested in a separate model study. The Lal and Peters (1967) source is represented as a function of latitude and altitude (pressure) and does not vary with season (see Figure 1 of Koch et al., 1996). No interannual variability in the ^{7}Be source is considered in the model (Liu et al., 2001). This may lead to an underestimate of tropospheric ^{7}Be concentrations, especially at high latitudes during a solar minimum (or near minimum) year. Lal and Peters (1967) reported that the relative amplitude of the ^{7}Be production rate over a 11-year solar cycle is about 13% below 300 hPa at latitudes above 45 degree.

Because of the coarse horizontal resolution of the model (2° latitude by 2.5° longitude), the model representation of the topography at the site is poor. The elevation of Mt. Cimone in the model is only 298 m, whereas in reality the mountain is 2165 m (asl) high (Figure 1). For

this reason, the model output was not sampled at ground level, but at the gridbox corresponding to the elevation of the site. In order to see the sensitivity of model-observation comparisons to spatial sampling, the model was sampled not only for the grid corresponding to the latitude and longitude of Mt. Cimone, but also for the 8 adjacent grids. To better understand the sources and seasonality of radiotracers in the model, we examine model output not only for ^{210}Pb, ^{7}Be and their ratio ^{7}Be/^{210}Pb (an indicator of vertical transport [Koch et al., 1996]), which can be directly compared to the measurements taken at Mt. Cimone, but also for other radiotracers and quantities, e.g., ^{222}Rn, and ^{10}Be/^{7}Be (a STE tracer [Zanis et al., 2003]).

Year 2005 was chosen for analysis because of the availability of the observational data and model output at the time of this work. As discussed later, the seasonal behavior of ^{210}Pb and ^{7}Be radionuclides during year 2005 was "typical" for Mt. Cimone. Monthly averages of ^{210}Pb and ^{7}Be data at Mt. Cimone were calculated for comparison with model results. To better compare the seasonalities of ^{210}Pb and ^{7}Be between the model and the observations, the monthly percentage deviations from the annual mean concentration were also calculated.

3 Seasonal Variations of Transport and Precipitation at Mt. Cimone: Observations vs. Model Simulations

Mt. Cimone is the windiest meteorological station in Italy and the prevailing local winds blow from S-SW and N-NE directions (Ciattaglia, 1983; Ciattaglia et al., 1987; Colombo et al., 2000). The wind observations at Mt. Cimone during the period of 1998-2011, when radionuclide measurements were performed at the station (Tositti et al., 2014), agree with the climatology of local wind intensity and direction during the period of 1946-1999 as reported by the Italian Air Force (Colombo et al., 2000). N-NE directions are more significant during the cold period, and fluxes from SW are more typical of the warm period. While winds blowing from the S-SW sector generate a sea air inflow, a continental air inflow is observed when winds come from the N-NE sector (Ciattaglia et al., 1987).

However, when considering the lifetimes of ^{210}Pb (about one week) and ^{7}Be (about three weeks) aerosols (Liu et al., 2001), it is apparent that the regional and long-range transport has a much more important role than local transport. On a large scale, about 70% of background air masses reaching Mt. Cimone in the period of 1996-1998 came from Atlantic and Arctic areas, with a smaller contribution from the Mediterranean Basin and the eastern area, as estimated by Bonasoni et al. (2000). A more recent and extended study of advection patterns at Mt. Cimone (Brattich E. et al., "Advection patterns at the WMO-GAW station of Mt. Cimone: seasonality, trends, and influence on atmospheric composition", manuscript in preparation, 2016), analyzing clusters of 4-day kinematic back-trajectories calculated for the period of 1998-2011 with the HYSPLIT (HYbrid Single-Particle Lagrangian Integrated Trajectory) model driven by the NCEP/NCAR (National Center for Environmental Prediction/National Center for Atmospheric Research) meteorological reanalysis, shows that the air masses advected to Mt. Cimone (55%) arrive from the Western-Atlantic-North America sector, while the remaining air masses (from the Arctic, Eastern and Mediterranean Basin-Northern Africa) together represent 45% of trajectories. Seasonal transport to Mt. Cimone in the model is shown in Figure 2, representing winds at the elevation of Mt. Cimone (winds are weaker at the model bottom layer). In agreement with the description of advection patterns at the site, prevailing model winds (Figure 2) blow from the western-Atlantic sector. Slow summer winds suggest the stronger influence of regional/local transport at Mt. Cimone during the period (e.g., Lee et al., 2007; Marinoni et al., 2008; Tositti et al., 2013, 2014; Brattich et al., 2015).

In the model, Mt. Cimone appears to be in a location where there is a large horizontal gradient of wind (transport) during 2005. Long-range transport from Western Europe, North America and Arctic region prevail during the cold period, while regional transport appears more important in summer. The model is able to capture relevant features of pressure systems

and seasonal circulation patterns of the North Atlantic/Mediterranean/African region, such as the semi-permanent high pressure system located in the North Atlantic with different positions during different seasons (Bermuda/Azores high), a semi-permanent system of high pressure centered in northeastern Siberia during the colder half of the year (Siberian high), and the ITCZ in the summer/autumn season. However, due to the coarse resolution of the global meteorological reanalysis that we use to construct the model winds, the more than 50 local-scale wind systems present in the Mediterranean and surrounding regions are not resolved (Burlando, 2009). In northern Europe, in fact, there are approximately two main states for the atmosphere, the westerly or zonal flows modulated by the advection of Atlantic lows, and the long-lived blocking anticyclonic configurations over North Sea or Scandinavia (easterly) (Burlando et al., 2008).

In the Mediterranean region, the main cyclones during winter are essentially sub-synoptic lows triggered by the major North-Atlantic synoptic systems affected by the local topography of the Northern Mediterranean coast (Trigo et al., 2002), whereas in summer cyclones develop because of thermal effects, orography (e.g., the Atlas Mountains), and increase in low-level thermal gradients (Trigo et al., 2002; Campins et al., 2006). Again, due to the coarse resolution of the meteorological data we use, these sub-synoptic processes are not resolved. For instance, North-African lows and Sahara depressions (also referred to as Atlas lee depressions) and the resulting S-SW wind (Sirocco) (Reiter, 1975), potentially linked to ^{210}Pb variations at Mt. Cimone, appear to be an important feature missing in the degraded MERRA data, where they appear only during October/November. However, MERRA is able to capture the summertime north-north easterly winds in the eastern Mediterranean (Aegean Sea), known as the Etesian winds, generated by thermal effects.

We evaluate the MERRA precipitation with those from the GPCP (Global Precipitation Climatology Project, http://www.gewex.org/gpcp.html) satellite and surface observations in

2005. Figure 3 shows the MERRA and GPCP monthly precipitation for the region defined by 0-75°N and 90°W – 90°E. A good agreement between the MERRA and the GPCP precipitations averaged over the region was found. In particular, summer precipitation patterns are very similar. The geographical distribution of precipitation in MERRA shows some important features in agreement with the observed climatology precipitations: the desert climate in North Africa with very low precipitation all year long, the ITCZ with high precipitation during the summer/autumn seasons, the North Atlantic region with high precipitation especially during the winter and autumn seasons, and Europe where the seasonal pattern of precipitation is similar to that in the North Atlantic region, but precipitation is lower.

Figure 4 shows the comparison of the GPCP and MERRA precipitation seasonality at Mt. Cimone. Since Mt. Cimone is located in a region with a large horizontal gradient in precipitation, we also show in the figure the comparisons for three adjacent gridboxes. The MERRA precipitation is generally lower than that of GPCP at two gridboxes (except for summer, Figure 4ab), but in good agreement at the other two gridboxes (Figure 4cd). The agreement between the MERRA and GPCP precipitation seasonality is reasonable, with the squared correlation coefficient R^2 varying between 0.56 (at the grid to the northwest of "ij") and 0.89 (at the grid to the southeast of "ij"). Large differences between the MERRA precipitation and that locally observed at the station are instead present. While the daily mean observed 2005 precipitation is 0.81 mm, which is close to the corresponding precipitation (0.73 mm) in MERRA at the "ij" grid (i.e., a negative bias of -0.08 mm); the model bias is positive and much higher (0.31 – 1.28 mm) at adjacent grids. This bias may very well reflect again the fact that the observed surface precipitation is localized, whereas the satellite and MERRA precipitations correspond to a much larger scale (about 200 km). Moreover, as Colombo et al. (2000) previously pointed out, different from the surrounding area where the climate is defined as temperate-continental, the climate at the mountaintop is classified as alpine because of the

high elevation. In fact, in agreement with the GPCP precipitation in 2005, the observed climatology in the region shows maximum during November (secondary maximum in spring) and absolute minimum in July (secondary minimum in January), whereas on the top of the mountain the precipitation is maximal during summer. The MERRA precipitation shows increased amounts during April and August-December, with minimum in June-July. As the local precipitation at the site is important to the scavenging of radionuclide aerosol tracers, this difference between the local and regional precipitation could contribute to any biases in our simulations. However, as we will show below, the ratio $^{7}Be/^{210}Pb$ may cancel out the errors associated to precipitation scavenging (Koch et al., 1996).

Low ^{210}Pb concentrations are seen over the Atlantic Ocean, due to the negligible emissions of ^{222}Rn from the oceans and strong precipitation scavenging, and in northern and western Europe especially during the cold season (Figure 2a). High ^{210}Pb concentrations appear over the Sahara Desert and North Africa, as a result of low precipitation in this area, and also over the Middle East and South Asia. ^{210}Pb concentrations over southern Europe appear higher during the transition seasons, especially fall, and peak during summer when the minimum precipitation and slow winds from west are observed in the region. Low ^{7}Be concentrations are simulated along the equator where convective scavenging is strongest (Figure 2b). High ^{7}Be concentrations are seen over the Sahara Desert due to a combination of low precipitation and subsidence in this region. Elevated values also occur over the Middle East, North America, and Greenland. ^{7}Be concentrations over southern Europe appear higher during spring and peak during winter, when model winds are stronger and transport ^{7}Be aerosols from North America and Greenland regions where ^{7}Be production is highest (Beer et al., 2012).

4 Seasonal Variations of ^{210}Pb and ^{7}Be at Mt. Cimone: Observations vs. Model Simulations

The seasonality and frequency distributions of ^{210}Pb and ^{7}Be concentrations measured at the Mt. Cimone station were previously examined by Lee et al. (2007), while more recent analyses of the 12-year record were presented in Tositti et al. (2014) and Brattich et al. (2015). Generally, both radionuclides show a marked seasonal maximum in the summertime, a behaviour shared by PM_{10} (Tositti et al., 2013) and O_3 (Bonasoni et al., 2000b). ^{210}Pb summer maximum is mainly due to the higher mixing height and enhanced uplift from the boundary layer as a result of thermal convection. The seasonal fluctuation of ^{7}Be is more complex and characterized by two relative maxima, one during the cold season associated with stratosphere-to-troposphere transport, and the other during the warm season mainly associated with tropospheric subsidence balancing lower-tropospheric air masses ascent occasionally accompanied by STE (Tositti et al., 2014). The ^{210}Pb and ^{7}Be measurements in 2005 are consistent with this description (Figure 5): ^{210}Pb concentrations are characterized by two maxima during the warm period (July and September); ^{7}Be concentrations are characterized by one absolute maximum during summer (July) and one secondary maximum during spring (March).

Figure 5 (ab) compares the simulated monthly ^{210}Pb and ^{7}Be activities with the observations at Mt. Cimone in 2005. The comparisons for the monthly percentage deviations from the annual mean concentration are available as Supplementary Information (hereafter SI, SI Figures 1-2). The seasonality of ^{210}Pb is well captured by the model. The model reproduces the presence of two seasonal maxima in the ^{210}Pb observations, with the maximum observed in July shifted to June in the simulation. The squared correlation coefficient R^2 between observed and simulated ^{210}Pb activities is equal to 0.83 at the "ij" grid and varies between 0.42 and 0.82 for adjacent gridboxes (to the north and to the west of "ij", respectively), confirming the good performance of the model in reproducing the ^{210}Pb seasonal pattern.

As for ^{7}Be, the model well captures the March maximum (i.e., secondary maximum in the observations) and the month-to-month variation during the cold and transition seasons (January-April, October-December). However, during the warm period, the simulated ^{7}Be concentrations are lower by a factor of 2 than the observed. A better agreement was found at some adjacent model gridboxes (e.g., to the south and to the southwest of "ij"; Figure 6 vs. Figure 5). The correlation between observed and simulated monthly ^{7}Be activities also increases from R^2 = 0.03 at "ij" to R^2 = 0.11-0.60 at adjacent model gridboxes. The largest value of R^2 = 0.6 was obtained at the "ij-1" gridbox to the south of "ij" (Figure 6). This improvement is due to the large horizontal gradient in the simulated ^{7}Be concentrations near the site (Figure 2).

5 Sources and Seasonality of ^{210}Pb and ^{7}Be at Mt. Cimone: A Model Analysis

In this section, we quantify the sources of ^{210}Pb and ^{7}Be and determine the processes governing their seasonality in the GMI model. Additional tracers as simulated by the model are used to aid in the interpretation. Model sensitivity experiments are conducted to examine the roles of transport and precipitation scavenging in the seasonality.

As discussed in Section 4, the model well reproduces the ^{210}Pb seasonality, with minimum in the cold period and maximum in the warm period. The ^{210}Pb seasonality (Figure 5a) can be linked with the seasonal pattern of its precursor ^{222}Rn (Figure 5c). It is seen that the summer ^{210}Pb maximum is due to stronger (thermal) convection, which uplifts more ^{222}Rn out of the boundary layer (e.g., Lee et al., 2007; Tositti et al., 2014; Brattich et al., 2015). This uplift of ^{222}Rn from the boundary layer is minimum in the cold period, and the minimal level of ^{210}Pb in this period can be considered representative of the free troposphere. The ^{210}Pb summer increase appears to be associated with short-range and regional transport, as suggested by the model simulations (Figure 2a). As expected, long-range transport is more typical of the

winter/spring seasons because of stronger horizontal winds, while regional effects are more important during summer when convection gets stronger.

In a similar manner, the source of the ^{7}Be March maximum can be investigated with model tracer simulations. Figure 5 (de) also shows the simulated seasonal patterns of the ^{10}Be/^{7}Be activity ratio and of the fraction of ^{7}Be originating from the stratosphere (strat ^{7}Be/total ^{7}Be). The simulated seasonal pattern of the ^{10}Be/^{7}Be ratio is very similar to the observations at Jungfraujoch (Switzerland, 3580 m asl) (Zanis et al., 2003), characterized by a clear seasonal cycle with peak ratios in spring. The usefulness of ^{10}Be/^{7}Be ratio as a stratospheric tracer is due to the fact that both ^{10}Be and ^{7}Be cosmogenic radionuclides attach to the same aerosols and share therefore the same removal mechanism. Moreover, due to the much longer physical half-life of ^{10}Be ($\tau_{1/2} = 1.5 \times 10^{6}$ years) compared to ^{7}Be ($\tau_{1/2} = 53.3$ days), their concentration ratios in the stratosphere (about 3-4) are much higher than in the troposphere (about 2 or even less) (Koch and Rind, 1998). The simulated ^{10}Be/^{7}Be ratio behavior indicates that deep stratosphere-to-troposphere (STT) peaks during winter, while shallower STT has a spring maximum, consistent with previous analyses of stratospheric intrusions at Mt. Cimone (Cristofanelli et al., 2006, 2009), and more generally with the climatology of stratosphere-troposphere exchange at the Northern Hemisphere mid-latitudes (James et al., 2003). Altogether the simulated high strat ^{7}Be/total ^{7}Be, high ^{7}Be/^{210}Pb (Figure 7), and low ^{10}Be/^{7}Be ratios during December-January indicate strongest STE during this period, followed by spring with slightly weaker stratospheric influence on surface ^{7}Be. However, the model tends to overestimate the observed ^{7}Be concentrations and ^{7}Be/^{210}Pb ratios during December-February, suggesting that stratospheric influence and/or subsidence in the model is probably too strong in this region at this time of the year. It is noted that globally integrated STT mass fluxes in the MERRA reanalysis are actually smaller than in some other reanalyses, e.g., ERA-Interim, JRA-55, and MERRA-2 (Boothe and Homeyer, 2016).

The use of the ^{7}Be production rate of Lal and Peters (1967) for a solar maximum year (1958) may partly explain the lower annual mean ^{7}Be in the model (3.4 mBq m^{-3} annual mean at the "ij" grid) than in the observations (4.2 mBq m^{-3}). In fact, the sunspot number in 2005 (29.8) was quite low (slowly decreasing from 2000, a solar maximum year, and reaching minimum in 2008), especially compared to the 1958 value of 184.8. Sunspot number data are available from the World Data Center for the production, preservation and dissemination of the international sunspot number (Sunspot Index and Long-term Solar Observation, SILSO, Royal Observatory of Belgium, Brussels, http://sidc.oma.be/sunspot-data/).

During the winter period, associated with the simulated and observed ^{7}Be increases (Figures 5-6), strong long-range transport was dominant in the European region (Figure 2b). Transport from higher latitude regions (Arctic, northern Europe, and North America) appears particularly important during this period (Figure 2b); such transport from high-latitude regions, where the ^{7}Be production rate is highest (Beer et al., 2012), has typically been observed during STE events at Mt. Cimone in many studies (e.g., Bonasoni et al., 1999, 2000ab).

The discrepancy between the simulated and the observed ^{7}Be concentrations during the warm period is partly due to the sensitivity to spatial sampling in the model. As seen from the map plots of ^{210}Pb and ^{7}Be concentrations at the elevation of Mt. Cimone (Figure 2), the sampling site appears to be located in a region where the N-S gradient of concentrations is large (especially for ^{7}Be). An elevated gradient in the region surrounding Mt. Cimone was also seen for winds, as transport plays a critical role in determining the distributions of these tracers. The sensitivity to spatial sampling in the model is therefore ascribed to this observed strong gradient in the N-S direction. In fact, while the grids to the south and southwest of "ij" are better for summer ^{7}Be comparisons (Figure 6), the grids to the northeast, north, and northwest of "ij" are better for winter (not shown).

The model underestimate of ^{7}Be levels in the warm months may also suggest the mixing of air masses between the PBL and the lower free troposphere is likely too weak. Previous observational analyses indicated that such mixing is higher in summer at Mt. Cimone due to enhanced convection and mountain wind breeze (e.g., Fischer et al., 2003; Cristofanelli et al., 2007). Weaker entrainment of free-tropospheric air into the PBL would result in lower ^{7}Be concentrations at the surface.

The model annual average biases are about 8% for ^{210}Pb and about 19% for ^{7}Be, respectively. By contrast, the model average bias for ^{7}Be/^{210}Pb ratios is about -13% (Figure 7). The smaller model bias for ^{7}Be/^{210}Pb ratios than for ^{7}Be concentrations reflects the fact that the ratio cancels out the errors in precipitation scavenging (Koch et al. 1996) that contribute to the underestimate of ^{210}Pb and ^{7}Be activities. On the other hand, the negative model bias for the ^{7}Be/^{210}Pb ratio again points to weak downward mixing from the free troposphere.

If one compares the month-to-month variation of ^{210}Pb and ^{7}Be (Figures 5 and 6) and precipitation in the model (Figure 4), the maxima/minima of precipitation appear to be in phase with those of both radionuclides' activities. This reflects the effects of precipitation scavenging on radionuclide aerosols.

We conducted model sensitivity experiments where convection (transport and scavenging), wet scavenging due to both large-scale and convective precipitation, and dry deposition processes are turned off, respectively, to examine the roles of these processes in controlling the seasonality of ^{210}Pb and ^{7}Be at Mt. Cimone. Figure 8 shows the results for the standard and sensitivity runs at the "grid to the south of "ij", for which the simulated tracer seasonal variations are similar to those observed, while the monthly percentage deviations from the annual mean concentrations are shown in SI Figure 3. Figures 9-12 show maps of simulated changes in ^{210}Pb and ^{7}Be concentrations when convection or wet scavenging is turned off.

Turning off dry deposition does not significantly change the simulated ^{210}Pb and ^{7}Be concentrations, partly due to sampling the higher vertical gridbox in the model (larger effects are seen at the bottom model layer). Turning off convection (i.e., with neither convective transport nor convective scavenging), the simulated ^{7}Be seasonality also remains nearly the same. This suggests the compensating effects between subsidence (increasing ^{7}Be) associated with convective transport and scavenging (decreasing ^{7}Be) due to convective precipitation. In the case of ^{210}Pb, turning off convection does not change the seasonal pattern but generally results in larger ^{210}Pb concentrations and particularly during summer/autumn when convective transport is more important at the site. In fact, no convective transport of ^{222}Rn (SI Figure 5) results in less ^{222}Rn (and ^{210}Pb) being transported to the free troposphere, but also more ^{210}Pb available in PBL lifted to the free troposphere by large-scale vertical transport; on the other hand, lack of convective scavenging of ^{210}Pb increases its concentration in the free troposphere. Turning off convection therefore results in an increase of ^{210}Pb concentrations in the free troposphere. Both surface ^{222}Rn concentrations at the elevation of Mt. Cimone (SI Figure 4), as well as a map of changes in ^{210}Pb concentrations due to convection in the model (Figure 9) show that convection in the region is more important during summer and autumn, but is not negligible during spring, possibly due to thermal inertia.

The model run without scavenging suggests that, apart from downward transport from the upper troposphere and lower stratosphere, wet scavenging is mainly responsible for the seasonal variation of ^{7}Be (Figure 8, bottom panel). None of our simulations is able to describe the observed ^{7}Be summertime peak, suggesting that local and regional circulations in this region with complex topography may not be resolved by the coarse-resolution model. For ^{210}Pb (Figure 8, top panel), it appears that wet scavenging plays a more important role during August-December than during January-July. This appears to be associated with the seasonality of precipitation, which shows prolonged elevated values during August-December, as well as a

maximum during April, as previously discussed (Figure 5). A plot of changes in ^{210}Pb concentrations due to scavenging in the model (Figure 10) confirms that the scavenging effect is larger during fall and, to a lesser extent, during summer. At Mt. Cimone, the scavenging effect is not minimal during July (month of minimum precipitation, Figure 4), suggesting the influence of precipitation scavenging elsewhere in the region on the site.

6 Summary and Conclusions

We have used a global 3-D model (GMI CTM) driven by the MERRA assimilated meteorological data from NASA's GMAO to simulate the ^{210}Pb and ^{7}Be observations from the Mt. Cimone (44°12' N, 10°42' E, 2165 m asl, Italy) WMO-GAW station in 2005. The two natural atmospheric radionuclides originate from contrasting source regions (lower troposphere and upper troposphere/lower stratosphere, respectively), attach to submicron particles, and are removed from the troposphere mainly by wet deposition. Our objective was to examine the roles of horizontal advection, vertical transport (large-scale and convection), and wet scavenging in determining the seasonality of ^{210}Pb and ^{7}Be at Mt. Cimone. The observed ^{210}Pb concentrations are characterized by maxima in summer and minima during the cold period. The seasonality of ^{7}Be is more complex, with a major peak in summer, a secondary peak in spring and a minimum in winter. This is the first modeling study of ^{210}Pb and ^{7}Be observations at Mt. Cimone. This site is representative of free-tropospheric Southern Europe/Mediterranean conditions most of the year, and as such the comparison between measurements and simulations can serve as an indication of shortcomings in the model or in the meteorological data.

Precipitation and wind fields are important to the model's performance in representing the transport and scavenging processes. We evaluated the MERRA precipitation field used by GMI CTM against the GPCP satellite and surface observations, and a generally good agreement was found. The seasonality of precipitation at Mt. Cimone shows increased amounts

during April and the period of August-December, and minimum in June-July. The MERRA assimilated winds at the low-resolution version we used captured the main circulation patterns (e.g., location of the Azores high pressure, location of the ITCZ) in the Northern Hemisphere. However, some local-scale winds and pressure systems, which are important for transport to the sampling site, were likely not well resolved at the coarse resolution we used. A general good agreement was found between the MERRA assimilated wind fields and the main advection patterns at the site (e.g., prevalence of long-range transport from Western Europe, North America and Arctic region during the cold season, as opposed to the prevailing regional transport during the warm season).

The model well reproduced the observed ^{210}Pb seasonality: ^{210}Pb maxima during the warm period were attributed to the stronger (thermal) convection, which uplifts more ^{222}Rn (and ^{210}Pb) from the boundary layer. The model is less successful in reproducing the observed ^{7}Be seasonality. ^{7}Be was better represented during the cold period, while the observed summer ^{7}Be maximum was underestimated by the model. The model underestimate of ^{7}Be levels in the warm months is partly due to the sensitivity to spatial sampling in the model, but also suggests that the mixing of air masses between the PBL and the lower free troposphere (e.g., via convection and compensating subsidence) is likely too weak during summer when the Mt. Cimone station is located within the PBL. This suggests that additional work comparing the model results with more surface observations is needed in order to better understand this effect. The simulated lower annual average ^{7}Be concentration relative to the observation is also partly attributed to the fact that the model used the ^{7}Be production rate for a solar maximum year, while in 2005 (our simulation year) the solar activity was rather low.

By examining the wind fields and horizontal distribution of radiotracers in the model, we noted that the sampling site is in a location where there is a large gradient, especially in the North-South direction. Accordingly, we investigated the sensitivity of model results to spatial

sampling. A better agreement between the model and the observations at some adjacent gridboxes was found. The ^{7}Be March maximum was linked to the large stratospheric influence during winter/spring. The model tends to underestimate the summertime ^{210}Pb and ^{7}Be, but better simulates the ^{7}Be/^{210}Pb ratio because the model errors due to precipitation scavenging appear to be canceled out in the ratio.

We have conducted a series of model sensitivity experiments to further examine and quantify the roles of wet scavenging, dry deposition, and convection (transport and scavenging) in controlling the seasonality of ^{210}Pb and ^{7}Be at Mt. Cimone. Dry deposition does not have a significant effect on the magnitude and seasonality of ^{210}Pb and ^{7}Be concentrations at the site. The relatively weak combined effects of convective transport and convective scavenging on the radiotracer seasonality were attributed to the compensating effects of convective transport and convective scavenging on tracer concentrations in the lower free troposphere (at the elevation of Mt. Cimone). Convection appears to be more important to the regional distribution of both radiotracers during summer and autumn, although it is also significant during spring. Finally, scavenging is found to be the most important process controlling the seasonal variations of ^{210}Pb and ^{7}Be at Mt. Cimone. For ^{210}Pb, precipitation plays a more important role during August-December than during January-July. This was attributed to the seasonality of local and regional precipitation, which shows prolonged elevated values in the period of August-December.

While our simulations demonstrated some capabilities of the model to reproduce the seasonality of ^{210}Pb and ^{7}Be, they highlight the weaknesses of the model in reproducing local features, presumably due to its coarse resolution. Model simulations at a higher resolution would improve this model analysis of ^{210}Pb and ^{7}Be observations at Mt. Cimone, a high-elevation site. The understanding of downward transport associated with convection during summer also requires improving. As such, ^{210}Pb and ^{7}Be tracers will prove to be very useful in

our understanding of seasonal behaviors of other environmentally important trace gases and aerosols at Mt. Cimone. Since other aerosols and trace gases (e.g., black carbon, CO, O_3) are also measured at the station, we plan to conduct comparisons between model simulations and those measurements to corroborate or contrast with the radionuclide results.

Data availability

A description of the observational data and model output used in this paper can be found in Sect. 2 and they are available upon request by contacting Laura Tositti (laura.tositti@unibo.it) and Hongyu Liu (hongyu.liu-1@nasa.gov), respectively.

Acknowledgements. Italian Air Force Meteorological Office (IAFMS) and ISAC-CNR are gratefully acknowledged for their precious technical support at the Mt. Cimone station. In particular, ISAC-CNR is gratefully acknowledged for providing infrastructural access at the WMO-GAW Global Station Italian Climate Observatory "O. Vittori" at Mt. Cimone. IAFMS is gratefully acknowledged for providing meteorological observations at Mt. Cimone station. The Italian Climate Observatory "O. Vittori" is supported by MIUR and DTA-CNR throughout the Project of National Interest NextData. Erika Brattich thanks the National Institute of Aerospace (NIA) Visitor Program for hosting her one month visit, and the Department of Biological, Geological and Earth Sciences of the University of Bologna for grant support during her PhD study. Hongyu Liu is supported by NASA Modeling and Analysis Program (MAP), NASA Atmospheric Composition Modeling and Analysis Program (ACMAP), and NASA Atmospheric Composition Campaign Data Analysis and Modeling (ACCDAM) program. The GMI activity is managed by José Rodriguez and Susan Strahan (NASA GSFC). Stephen Steenrod, Megan Damon, and Jules Kouatchou (GSFC) are acknowledged for

programming support. NASA Center for Computational Sciences (NCCS) provided supercomputing resources.

References

Arimoto, R., Snow, J.A., Graustein, W.C., Moody, J.L., Ray, B.J., Duce, R.A., Turekian, K.K., and Maring H.B.: Influences of atmospheric transport pathways on radionuclide activities in aerosol particles from over the North Atlantic, J Geophys Res, 104(D17), 301-321, 1999.

Balkanski, Y, Jacob, D.J., Gardner, G.M., Graustein, W., Turekian, K.K.: Transport and residence times of tropospheric aerosols inferred from a global three-dimensional simulation of ^{210}Pb, J Geophys Res, 98 (D11), 20573-20586, 1993.

Baskaran, M.: Po-210 and Pb-210 as atmospheric tracers and global atmospheric Pb-210 fallout: a review, J Environ Radioactiv, 102, 500-513, 2011.

Beer, J., McCracken, K., and von Steiger, R.: Cosmogenic radionuclides. Springer, Heidelberg, Germany, 2012.

Bonasoni, P., Evangelisti, F., Bonafé, U., Feldmann, H., Memmesheimer, M., Stohl, A., and Tositti, L.: Stratosphere-troposphere exchanges: case studies recorded at Mt. Cimone during VOTALP project, Phys Chem Earth (C), 24(5), 443-446, 1999.

Bonasoni, P., Evangelisti, F., Bonafé, U., Ravegnani, F., Calzolari, F., Stohl, A., Tositti, L,. Tubertini, O., and Colombo, T.: Stratospheric ozone intrusion episodes recorded at Mt. Cimone during VOTALP project: Case studies, Atmos Environ, 34, 1355-1365, 2000a.

Bonasoni, P., Stohl, A., Cristofanelli, P., Calzolari, F., Colombo, T., and Evangelisti, F.: Background ozone variations at Mt Cimone station, Atmos Environ, 34, 5183-5189, 2000b.

Boothe, A. C. and Homeyer, C. R.: Global large-scale stratosphere-troposphere exchange in modern reanalyses, Atmos. Chem. Phys. Discuss., doi:10.5194/acp-2016-788, in review, 2016.

Bourcier, L., Masson, O., Laj, P., Pichon, J.M., Paulat, P., Freney, E., and Sellegri, K.: Comparative trends and seasonal variation of ^{7}Be, ^{210}Pb and ^{137}Cs at two altitude sites in the central part of France, J Environ Radioactiv, 102, 294-301, 2011.

Brattich, E., Hernandéz-Ceballos, M.A., Cinelli, G., and Tositti, L.: Analysis of peak ^{210}Pb values at Mt. Cimone (1998-2011), Atmos Environ, 112, 136-147, 2015.

Brattich, E., Orza, J.A.G., and Tositti, L.: Advection patterns at the WMO-GAW station of Mt. Cimone: seasonality, trends, and influence on atmospheric composition, manuscript in preparation, 2016.

Brost, R.A., Feichter, J., and Heimann, H.: Three-dimensional simulation of ^{7}Be in a global climate model, J Geophys Res, 96, 22423-22445, 1991.

Burlando, M.: The synoptic-scale surface wind climate regimes of the Mediterranean Sea according to the cluster analysis of ERA-40 wind fields, Theor Appl Climatol, 96, 69-83, 2009.

Burlando, M., Antonelli, M., and Ratto, C.F.: Mesoscale wind climate analysis: identification of anemological regions and wind regimes, Int J Climatol, 28, 629-641, 2008.

Caillet, S., Arpagaus, P., Monna, F., and Dominik, J.: Factors controlling ^{7}Be and ^{210}Pb atmospheric deposition as revealed by sampling individual rain events in the region of Geneva, Switzerland, J Environ Radioactiv, 53, 241-256, 2001.

Campins, J., Jansà, A., and Genovés, A.: Three-dimensional structure of western Mediterranean cyclones, Int J Climatol, 26, 323-343, 2006.

Cannizzaro, F., Greco, G., Raneli, M., Spitale, M.C., and Tomarchio, E.: Concentration measurements of ^{7}Be at ground level air at Palermo, Italy – comparison with solar activity over a period of 21 years, J Environ Radioactiv, 84, 457-467, 2004.

Carvalho, A.C., Reis, M., Silva, L., and Madruga, M.J.: A decade of ^{7}Be and ^{210}Pb activity in surface aerosols measured over the Western Iberian Peninsula, Atmos Environ, 67, 193-202, 2013.

Ciattaglia, L.: Interpretation of atmospheric CO2 measurements at Mt. Cimone (Italy) related to wind data. Journal of Geophysical Research 88, C2, 1331-1338, 1983.

Ciattaglia, L., Cundari, V., and Colombo, T.: Further measurements of atmospheric carbon dioxide at Mt. Cimone, Italy: 1979-1985, Tellus B, 39, 13-20, 1987.

Colombo, T., Santaguida, R., Capasso, A., Calzolari, F., Evangelisti, F., and Bonasoni, P.: Biospheric influence on carbon dioxide measurements in Italy, Atmos Environ, 34, 4963-4969, 2000.

Considine, D.B., Douglass, A.R., Connell, P.S., Kinnison, D.E., and Rotman, D.A.: A polar stratospheric cloud parameterization for the global modeling initiative three-dimensional model and its response to stratospheric aircraft, J Geophys Res, 105(D3), 3955-3973, 2000.

Considine, D.B., Connell, P.S., Logan, J.A.: Simulating ozone in the near tropopause region with a new combined model of the stratosphere and troposphere, in: Quadrennial Ozone Symposium QOS 2004, edited by: Zerefos, C, International Ozone Commission, Kos, Greece, pp. 739-740, 2004.

Considine, D.B., Bergmann, D.J., and Liu, H.: Sensitivity of Global Modeling Initiative chemistry and transport model simulations of radon-222 and lead-210 to input meteorological data, Atmos Chem Phys, 5, 3389-3406, 2005.

Cristofanelli, P., Bonasoni, P., Collins, W., Feichter, J., Forster, C., James, P., Kentarchos, A., Kubik, P.W., Land, C., Meloen, J., Roelofs, G.J., Siegmund, P., Sprenger, M., Schnabel, C., Stohl, A., Tobler, L., Tositti, L., Trickl, T., and Zanis, P.: Stratosphere-to-troposphere transport: A model and method evaluation, J Geophys Res, 108(D12), 8525, doi:10.1029/2002JD002600, 2003.

Cristofanelli, P., Bonasoni, P., Tositti, L., Bonafé, U., Calzolari, F., Evangelisti, F., Sandrini, S., and Stohl, A.: A 6-year analysis of stratospheric intrusions and their influence on ozone at Mt. Cimone (2165 m above sea level), J Geophys Res, 111, D03306, doi:10.1029/2005JD006553, 2006.

Cristofanelli, P., Bonasoni, P., Carboni, G., Calzolari, F., Casarola, L., Zauli Sajani, S., and Santaguida, R.: Anomalous high ozone concentrations recorded at a high mountain station in Italy in summer 2003, Atmos Environ, 41, 1383-1394, 2007.

Cristofanelli, P., Calzolari, F., Bonafé, U., Duchi, R., Marinoni, A., Roccato, F., Tositti, L., and Bonasoni P.: Stratospheric intrusion index (SI^2) from baseline measurement data, Theor Appl Climatol, 97, 317-325, 2009a.

Cristofanelli, P., Marinoni, A., Arduini, J., Bonafé, U., Calzolari, F., Colombo, T., Decesari, S., Duchi, R., Facchini, M.C., Fierli, F., Finessi, E., Maione, M., Chiari, M., Calzolai, G., Messina, P., Orlandi, E., Roccato, F., and Bonasoni, P.: Significant variations of trace gas composition and aerosol properties at Mt. Cimone during air mass transport from North Africa – contributions from wildfire emissions and mineral dust, Atmos Chem Phys, 9, 4603-4619, 2009b.

Cristofanelli, P., Scheel, H.-E., Steinbacher, M., Saliba, M., Azzopardi, F., Ellul, R., Fröhlich, M., Tositti, L., Brattich, E., Maione, M., Calzolari, F., Duchi, R., Landi, T.C., Marinoni, A., and Bonasoni, P.: Long-term surface ozone variability at Mt. Cimone WMO/GAW global station (2165 m a.s.l., Italy), Atmos Environ, 101, 23-33, 2015.

Cuevas, E., Gonzalez, Y., Rodríguez, S., Guerra, J.C., Gómez-Peláez, A.J., Alonso-Pérez, S., Bustos, J., and Milford, C.: Assessment of atmospheric processes driving ozone variations in the subtropical North Atlantic free troposphere, Atmos Chem Phys, 13, 1973-1998, 2013.

Daish, S.R., Dale, A.A., Dale, C.J., May, R., and Rowe, J.E.: The temporal variations of ^{7}Be, ^{210}Pb and ^{210}Po in England, J Environ Radioactiv, 84, 457-467, 2005.

Dibb, J.E., Talbot, R.W., and Gregory, G.L.: Beryllium 7 and lead 210 in the western hemisphere Arctic atmosphere: Observations from three recent aircraft-based sampling programs, J Geophys Res, 97, 16709-16715, 1992.

Dibb, J.E., Meeker, L.D., Finkel, R.C., Southon, J.R., Caffee, M.W., and Barrie, L.A.: Estimation of stratospheric input to the Arctic troposphere: ^{7}Be and ^{10}Be in aerosols at Alert, Canada, J Geophys Res, 99, 12855-12864, 1994.

Dibb, J.E.: Vertical mixing above Summit, Greenland: insights into seasonal and high frequency variability from the radionuclide tracers ^{7}Be and ^{210}Pb, Atmos Environ, 41, 5020-5030, 2007.

Dueñas, C., Fernández, M.C., Cañete, S., and Pérez, M.: ^{7}Be to ^{210}Pb concentration ratio in ground level air in Málaga (36.7°N, 4.5°W), Atmos Res, 92, 49-57, 2009.

Dueñas, C., Orza, J.A.G., Cabello, M., Fernández, M.C., Cañete, S., Pérez, M., and Gordo, E.: Air mass origin and its influence on radionuclide activities (^{7}Be and ^{210}Pb) in aerosol particles at a coastal site in the western Mediterranean, Atmos Res, 101, 205-214, 2011.

Duncan, B.N., Strahan, S.E., and Yoshida, Y.: Model study of the cross-tropopause transport of biomass burning pollution, Atmos Chem Phys, 7, 3713-3736, 2007.

Duncan, B.N., West, J.J., Yoshida, Y., Fiore, A.M., and Ziemke, J.R.: The influence of European pollution on ozone in the Near East and northern Africa, Atmos Chem Phys, 8, 2267-2283, doi:10.5194/acp-8-2267-2008, 2008.

Feely, H.W., Larsen, R.J., and Sanderson, C.G.: Factors that cause seasonal variations in beryllium-7 concentrations in surface air, J Environ Radioactiv, 9, 223-249, 1989.

Feichter, J., Brost, R.A., and Heimann, M.: Three-dimensional modeling of the concentration and deposition of ^{210}Pb aerosols, J. Geophys. Res., 96, 22 447-22 469, 1991.

Fischer, H., Kormann, R., Klüpfel, T., Gurk, C., Königstedt, R., Parchatka, U., Mühle, J., Rhee, T.S., Brenninkmeijer, C.A.M., Bonasoni, P., and Stohl, A.: Ozone production and trace gas

correlations during the June 2000 MINATROC intensive measurement campaign at Mt. Cimone. Atmos Chem Phys, 3, 725-738, 2003.

Forster, P., Ramaswamy, V., Artaxo, P., Berntsen, T., Betts, R., Fahey, D.W., Haywood, J., Lean, J., Lowe, D.C., Myhre, G., Nganga, J., Prinn, R., Raga, G., Schulz, M., and Van Dorland, R.: Changes in Atmospheric Constituents and in Radiative Forcing, in Climate Change 2007: The Physical Science Basis. Contribution of Working Group I to the Fourth Assessment Report of the Intergovernmental Panel on Climate Change, [Solomon, S., Qin, D., Manning, M., Chen, Z., Marquis, M., Averyt, K.B., Tignor, M., and Miller, H.L. (eds.)], Cambridge University Press, Cambridge, United Kingdom and New York, NY, USA, 2007.

Froehlich, K., and Masarik, J.: Radionuclides as tracers and timers of processes in the continental environment – Basic concepts and methodologies. In: Radioactivity in the Environment, 16, Chapter 2, 27-50, Environmental Radionuclides: Tracers and Timers of Terrestrial Processes. Edited by Elsevier. doi:10.1016/S1569-4860(09)01602-7, 2010

Gaffney, J.S, Marley, N., and Cunningham, M.M.: Natural radionuclides in fine aerosols in the Pittsburgh area, Atmos Environ, 38, 3191-3200, 2004.

Gäggeler, H.W.: Radioactivity in the atmosphere, Radiochim Acta, 70-71, 345-353, 1995.

Gerasopoulos, E., Zanis, P., Stohl, A., Zerefos, C.S., Papastefanou, C., Ringer, W., Tobler, L., Hübener, S., Gäggeler, H.W., Kanter, H.J., Tositti L., and Sandrini, S.: A climatology of ^{7}Be at four high-altitude stations at the Alps and the Northern Apennines, Atmos Environ, 35, 6347-6360, 2001.

Gerasopoulos, E., Zanis, P., Zerefos, C.S., Papastefanou, C., Ringer, W., Gäggeler, H.W., Tobler, L., and Kanter, H.J.: Factors and processes controlling the concentration of the cosmogenic radionuclide ^{7}Be at high-altitude Alpine stations, In: Radioactivity in the Environment, Volume 7, 863-870, Elsevier Ltd., ISSN 1569-4860, DOI10.1016/S1569-4860(04)07108-6, 2005.

Graustein, W.C., and Turekian, K.K.: Radon fluxes from soils to the atmosphere measured by ^{210}Pb-^{226}Ra disequilibrium in soils, Geophys Res Lett, 17, 841-844, 1990.

Graustein, W.C., and Turekian, K.K.: ^{7}Be and ^{210}Pb indicate an upper troposphere source for elevated ozone in the summertime subtropical free troposphere of the eastern North Atlantic, Geophys Res Lett, 23, 539-542, 1996.

Hötzl, H., and Winkler, R.: Activity concentrations of ^{226}Ra, ^{228}Ra, ^{210}Pb, ^{40}K and ^{7}Be and their temporal variations in surface air, J Environ Radioactiv, 5, 445-458, 1987

Huang M., Carmichael, G.R., Chai, T., Pierce, R.B., Oltmans, S.J., Jaffe, D.A., Bowman, K.W., Kaduwela, A., Cai, C., Spak, S.N., Weinheimer, A.J., Huey, L.G., and Diskin, G.S.: Impacts of transported background pollutants on summertime western US air quality: model evaluation, sensitivity analysis and data assimilation, Atmos Chem Phys, 13, 359-391, 2013.

Ioannidou, A., Manolopoulou, M., and Papastefanou, C.: Temporal changes of ^{7}Be and ^{210}Pb concentrations in surface air at temperate latitudes (40°), Appl Radiat Isotopes, 63(2), 277-284, 2005.

Ioannidou, A., Vasileiadis, A., and Melas, D.: Time lag between the tropopause height and ^{7}Be activity concentrations in surface air, J Environ Radioactiv, 129, 80-85, 2014.

Jacob, D.J., and Prather, M.J.: Radon-222 as a test of boundary layer convection in a general circulation model, Tellus B, 42, 118-134, 1990.

James, P., Stohl, A., Forster, C., Eckhardt, S., Seibert, P., and Frank, A., A 15-year climatology of stratosphere-troposphere exchange with a Lagrangian particle dispersion model 2. Mean climate and seasonal variability, J Geophys Res, 108(D12), 8522, doi:10.1029/2002JD002639, 2003.

Jasiulionis, R., and Wershofen, H.: A study of the vertical diffusion of the cosmogenic radionuclides, ^{7}Be and ^{22}Na in the atmosphere. J Environ Radioactiv, 79, 157-169, 2005.

Johnson, W., and Viezee, W., Stratospheric ozone in the lower troposphere: i. Presentation and interpretation of aircraft measurements. Atmos Environ, 15, 1309–1323, 1981.

Junge, C.E.: Air chemistry and radioactivity. Academic Press, New York, USA, and London, UK, 382 pp, 1963.

Kinnison, D.E., Connell, P.S., Rodriguez, J.M., Rotman, D.A., Considine, D.B., Tannahill, J., Ramaroson, R., Rasch, P.J., Douglass, A.R., Baughcum, S.L., Coy, L., Waugh, D.W., Kawa, S.R., and Prather, M.J.: The Global Modeling Initiative assessment model: Application to high-speed civil transport perturbation, J Geophys Res, 106(D2), 1693-1711, 2001.

Koch, D.M., Jacob, D.J., and Graustein, W.C.: Vertical transport of tropospheric aerosols as indicated by ^{7}Be and ^{210}Pb in a chemical tracer model, J Geophys Res, 101(D13), 18651-18666, 1996.

Koch, D., and Rind, D.: Beryllium10/beryllium7 as a tracer of stratospheric transport, J Geophys Res, 103, 3907-3917, 1998.

Kulan, A., Aldahan, A., Possnert, G., and Vintersved, I.: Distribution of ^{7}Be in surface air of Europe, Atmos Environ, 40, 3855-3868, 2006.

Lal, D., Malhotra, P.K., and Peters, B.: On the production of radioisotopes in the atmosphere by cosmic radiation and their application to meteorology, J Atmos Sol-Terr Phy, 12, 306-328, 2006.

Lal, D., and Peters, B.: Cosmic ray produced radioactivity on the Earth, in: Handbuch der Physik, 46/2, edited by Sitte, K., Springer-Verlag, New York, USA, pp. 551-561, 1967.

Lee, H. N., Wan, G., Zheng, X., Sanderson, C.G., Josse, B., Wang, S., Yang, W., Tang, J., and Wang, C.: Measurements of ^{210}Pb and ^{7}Be in China and their analysis accompanied with

global model calculations of ^{210}Pb, J Geophys Res, 109, D22203, doi:10.1029/2004JD005061, 2004.

Lee, H. N., Tositti, L., Zheng, X., and Bonasoni, P.: Analyses and comparisons of variations of ^{7}Be, ^{210}Pb and ^{7}Be/^{210}Pb with ozone observations at two Global Atmosphere Watch stations from high mountains, J Geophys Res, 112, D05303, doi:10.1029/2006JD007421, 2007

Lelieveld, J., Berresheim, H., Borrman, S., Crutzen, P.J., Dentener, F.J., Fischer, H., Feichter, J., Flatau, P.J., Heland, J., Holzinger, R., Korrmann, R., Lawrence, M.G., Levin, Z., Markowicz, K.M., Mihapoulos, N., Minikin, A., Ramanathan, V., de Reus, M., Roelofs, G.J., Scheeren, H.A., Sciare, J., Schlager, H., Schultz, M., Siegmund, P., Steil, B., Stephanou, E.G., Stier, P., Traub, M., Warneke, C., Williams, J., and Ziereis, H.: Global air pollution crossroads over the Mediterranean. Science, 298, 794-799, 2002.

Li, Q., Jacob, D.J., Logan, J.A., Bey, I., Yantosca, R.M., Liu, H., Martin, R.V., Fiore, A.M., Field, B.D., Duncan, B.N.: A Tropospheric Ozone Maximum Over the Middle East, Geophys Res Lett, 28(17), 3235-3238, 2001.

Likuku, A.S.: Factors influencing ambient concentrations of ^{210}Pb and ^{7}Be over the city of Edinburgh (55.9°N, 03.2°W), J Environ Radioactiv, 87, 289-304, 2006.

Liu, H., Jacob, D.J., Bey, I., and Yantosca, R.M.: Constraints from the ^{210}Pb and ^{7}Be on wet deposition and transport in a global three-dimensional chemical tracer model driven by assimilated meteorological fields, J Geophys Res, 106, D11, 12109-12128, 2001.

Liu, H., Jacob, D.J., Dibb, J.E., Fiore, A.M., and Yantosca, R.M.: Constraints on the sources of tropospheric ozone from ^{210}Pb-^{7}Be-O_3 correlations, J Geophys Res, 109(D07306), doi:10.1029/2003JD003988, 2004.

Liu, H., Considine, D. B., Horowitz, L. W., Crawford, J. H., Rodriguez, J. M., Strahan, S. E., Damon, M. R., Steenrod, S. D., Xu, X., Kouatchou, J., Carouge, C., and Yantosca, R. M.:

Using beryllium-7 to assess cross-tropopause transport in global models, Atmos. Chem. Phys., 16, 4641-4659, doi:10.5194/acp-16-4641-2016, 2016.

Lozano, R.L., Hernandéz-Ceballos, M.A., San Miguel, E.G., Adame, J.A., and Bolívar, J.P.: Meteorological factors influencing the ^{7}Be and ^{210}Pb concentrations in surface air from the southwestern Iberian Peninsula, Atmos Environ, 63, 168-178, 2012.

Lozano, R.L., Hernandéz-Ceballos, M.A., Rodrigo, J.F., San Miguel, E.G., Casas-Ruiz, M., García-Tenorio, R., and Bolívar, J.P.: Mesoscale behavior of ^{7}Be and ^{210}Pb in superficial air along the Gulf of Cadiz (south of Iberian peninsula), Atmos Environ, 80, 75-84, 2013.

Marinoni, A., Cristofanelli, P., Calzolari, F., Roccato, F., Bonafé, U., and Bonasoni, P.: Continuous measurements of aerosol physical parameters at the Mt. Cimone GAW Station (2165 m asl, Italy), Sci Total Environ, 391, 241-251, 2008.

Millàn, M., Sanz, J., Salvador, R., and Mantilla, E.: Atmospheric dynamics and ozone cycles related to nitrogen deposition in the western Mediterranean, Environ Pollut, 118, 167-186, 2006.

Monks, P.S., Granier, C., Fuzzi, S., Stohl, A., Williams, M.L., Akimoto, H., Amann, M., Baklanov, A., Baltensperger, U., Bey, I., Blake, N., Blake, R.S., Carslaw, K., Cooper, O.R., Dentener, F., Fowler, D., Fragkou, E., Frost, G.J., Generoso, S., Ginoux, P., Grewe, V., Guenther, A., Hansson, H.C., Henne, S., Hjorth, J., Hofzumahaus, A., Huntrieser, H., Isaksen, I.S.A., Jenkin, M.E., Kaiser, J., Kanakidou, M., Klimont, Z., Kulmala, M., Laj, P., Lawrence, M.G., Lee, J.D., and Liousse, C.: Atmospheric composition change – global and regional air quality, Atmos Environ, 43, 5268-5350, 2009.

Moore, H.E., Poet, S.E., and Martell, E.A.: ^{222}Rn, ^{210}Pb, ^{210}Bi, and ^{210}Po, profiles and aerosol residence times versus altitude, J Geophys Res, 78, 7065-7075, 1973.

Nazaroff, W.W.: Radon transport from soil to air, Rev Geophys, 30, 137-160, 1992.

ORTEC: Gamma-Vision 32 A66-B32 user's manual. ORTEC USA, Part No. 783620, Manual Revision D, 2003.

Papastefanou, C., and Ioannidou, A.: Aerodynamic size association of ^{7}Be in ambient aerosols. J Environ Radioactiv, 26, 273-282, 1995.

Pham, M.K., Betti, M., Nies ,H., and Povinec, P.P.: Temporal changes of ^{7}Be, ^{137}Cs and ^{210}Pb activity concentrations in surface air at Monaco and their correlation with meteorological parameters, J Environ Radioactiv, 102, 1045-1054, 2011.

Rastogi, N., and Sarin, M.M.: Atmospheric ^{210}Pb and ^{7}Be in ambient aerosols over low- and high-altitude sites in 34 semiarid region: Temporal variability and transport processes, J Geophys Res, 113, doi:10.1029/2007JD009298, 2008.

Rehfeld, S., and Heimann, M.: Three dimensional atmospheric transport simulation of the radioactive tracers ^{210}Pb, ^{7}Be, ^{10}Be, and ^{90}Sr, J Geophys Res, 100 (D12), 26141-26161, 1995.

Reiter, E.R.: Weather phenomena of the Mediterranean basin. Part 1. General description of the meteorological processes, In: Handbook for forecasters in the Mediterranean basin, Environment Prediction Research Facility, Naval Postgraduate School, Monterey, California, U.S. Department of Commerce, available at http://www.dtic.mil/cgi-bin/GetTRDoc?AD=ADA024271, last accessed 15 March 2016, 1975.

Reiter, R., Sladkovich, K., Pötzl, K., Carnuth, W., and Kanter H.J.: Studies on the influx of stratospheric air into the lower troposphere using cosmic-ray produced radionuclides and fallout, Arch Meteor Geophy A, Vol.20(3), 211-246, 1971.

Reiter, R., Munzert, K., Kanter, H.-J., and Pötzl, K.: Cosmogenic radionuclides and ozone at a mountain station at 3.0 km a.s.l., Arch Meteor Geophy B, 32, 131-160, 1983.

Rienecker, M.M., Suarez, M.J., Gelaro, R., Todling, R., Bacmeister, J., Liu, E., Bosilovich, M.G., Schubert, S.D., Takacs, L., Kim, G.-K., Bloom, S., Chen, J., Collins, D., Conaty, A.,

da Silva, A., Gu, W., Joiner, J., Koster, R.D., Lucchesi, R., Molod, A., Owens, T., Pawson, S., Pegion, P., Redder, C.R., Reichle, R., Robertson, F.R., Ruddick, A.G., Sienkewicz, M., and Woollen, J.: MERRA: NASA's Modern-Era Retrospective Analysis for Research and Applications. J Climate, 24(14), 3624-3648, 2011.

Rodriguez, J.M., Logan, J.A., Bergmann, D., Megretskaia, I., Jacob, D.J., Xie, H., Das, B., and Strahan, S.E.: The impact of meteorological fields on tropospheric ozone distributions calculated by the Global Modeling Initiative (GMI) chemical-transport model, in: Quadrennial Ozone Symposium QOS 2004, edited by: Zerefos, C., pp.147, International Ozone Commission, Kos, Greece, 2004

Rotman, D.A., Tannahill, J.R., Kinnison, D.E., Connell, P.S., Bergmann, D., Proctor, D., Rodriguez, J.M., Lin, S.J., Rood, R.B., Prather, M.J., Rasch, P.J., Considine, D.B., Ramaroson, R., and Kawa, S.R.: Global Modeling Initiative assessment model: Model description, integration, and testing of the transport shell, J Geophys Res, 106(D2), 1669-1691, 2001.

Schery, S.D., Whittlestone, S., Hart, K.P., and Hill, S.E.: The flux of radon and thoron from Australian soils, J Geophys Res, 100, 26141-26161, 1989.

SILSO (Sunspot Index and Long-term Solar Observation), World Data Center – Sunspot Number and Long-Term Solar Observations, Royal Observatory of Belgium, on-line Sunspot Number catalogue, available at http://sidc.oma.be/silso/, last accessed 15 March 2016

Simon, J., Meresova, J., Sykora, I., Jeskovsky, M., and Holy, K.: Modeling of temporal variations of vertical concentration profile of ^{7}Be in the atmosphere. Atmos Environ, 43, 2000-2004, 2009.

Steinmann, P., Zeller, M., Beuret, P., Ferreri, G., and Estier, S.: Cosmogenic ^{7}Be and ^{22}Na in ground level air in Switzerland (1994-2011), J Environ Radioactiv, 124, 68-73, 2013.

Stohl, A., Wernli, H., James, P., Borqui, M., Forster, C., Liniger, M.A., Seibert, P., and Sprenger, M.: A new perspective of stratosphere-troposphere exchange, Bull Am Meteor Soc, 84, 1565-1573 DOI: 10.1175/BAMS-84-11-1565, 2003.

Strahan, S.E., Duncan, B.N., and Hoor, P.: Observationally-derived diagnostics of transport in the lowermost stratosphere and their application to the GMI chemistry transport model. Atmos Chem Phys, 7, 1435-2445, 2007

Todorovic, D., Popovic, D., Djuric, G., Radenkovic, M.: ^{7}Be to ^{210}Pb concentration ratio in ground level air in Belgrade area, J Environ Radioactiv, 79, 297-307, 2005.

Tositti, L., Riccio, A., Sandrini, S., Brattich, E., Baldacci, D., Parmeggiani, S., Cristofanelli, P., and Bonasoni, P.: Short-term climatology of PM10 at a high altitude background station in southern Europe, Atmos Environ, 65, 145-152, 2013.

Tositti, L., Brattich, E., Cinelli, G., and Baldacci, D.: 12 years of ^{7}Be and ^{210}Pb data in Mt. Cimone, and their correlation with meteorological parameters, Atmos Environ, 87C, 108-122. doi: 10.1016/j.atmosenv.2014.01.014, 2014.

Trickl, T., Feldmann, H., Kanter,H.-J., Scheel, H.-E., Sprenger, M., Stohl, A. and Wernli, H., 2010. Forecasted deep stratospheric intrusions over central Europe: case studies and climatologies, Atmos Chem Phys, 10, 499-524.

Trigo, I.F., Bigg, G.R., and Davies, T.D.: Climatology of cyclogenesis mechanisms in the Mediterranean. Mon Weather Rev, 130, 549-569, 2002.

Turekian, K.K., Nozaki, Y., and Benninger, L.K.: Geochemistry of atmospheric radon and radon products. Annu Rev Earth Pl Sc, 5, 227-255, 1977.

Turekian, K.K., and Graustein, W.C.: Natural Radionuclides in the Atmosphere, in: Treatise on Geochemistry, Volume 4, Ralph Keeling, F. (Ed.), Holland, H.D., and Turekian, K.K. (executive editors), pp. 347, doi:10.1016/B0-08-043751-6/04042-1, ISBN 0-08-043751-6. Elsevier, p.261-279, 2003.

Usoskin, I., and Kovaltsov, G.: Production of cosmogenic ^{7}Be isotope in the atmosphere: full 3D modelling. J Geophys Res, 113, D12107, 2008.

van Dingenen, R, Putaud, J.P., Martins-Dos Santos, S., Raes, F. Physical aerosol properties and their relation to air mass origin at Monte Cimone (Italy) during the first MINATROC campaign, Atmos Chem Phys, 5, 2203-2226, 2005.

Viezee, W., and Singh, H.B.: The distribution of beryllium-7 in the troposphere. Implications on stratosphere/tropospheric air exchange, Geophys Res Lett, 7, 805-808, 1980.

Wilkening, M.H., Clements, W.E., and Stanley, D.: Radon222 flux measurements in widely separated regions, In: The Natural Radiation Environment II, pp. 717-730, U.S. Energy and Res. Dev. Admin., Oak Ridge, Tenn, USA, 1975.

Winkler, R., Dietl, F., Frank, G., and Thiersch, J.: Temporal variation of ^{7}Be and ^{210}Pb size distributions in ambient aerosols, Atmos Environ, 32, 983-991, 1998.

WMO-GAW (World Meteorological Organization - Global Atmosphere Watch): 1st International Expert Meeting on Sources and Measurements of Natural Radionuclides Applied to Climate and Air Quality Studies, (Gif-sur-Yvette, France, 3-5 June 2003) (WMO TD No. 1201), Report No. 155 [available at ftp://ftp.wmo.int/Documents/PublicWeb/arep/gaw/gaw155.pdf, last accessed 15 March 2016], 2004

Zanis, P., Schuepbach, E., Gäggeler, H.W., Huebener, S., and Tobler, L.: Factors controlling Beryllium-7 at Jungfraujoch in Switzerland, Tellus, 51 (4), 789-805, 1999.

Zanis, P., Monks, P.S., Schuepbach, R., Carpenter, L.J., Green, T.J., Mills, G.P, Bauguitte, S., and Penkett, S.A.: In situ ozone production under free tropospheric conditions during FREETEX '98 in the Swiss Alps, J Geophys Res, 105 (D1), 24223-24234, 2000.

Zanis, P., Gerasopoulos, E., Priller, A., Schnabel, C., Stohl, A., Zerefos, C., Gäggeler, H.W., Tobler, L., Kubik, P.W., Kanter, H.J., Scheel, H.E., Luterbacher, J., and Berger, M.: An

estimate of the impact of stratosphere-to-troposphere transport (STT) on the lower free tropospheric ozone over the Alps using ^{10}Be and ^{7}Be measurements, J Geophys Res, 108(D12), 8520, doi:10.1029/2002JD002604, 2003.

Figures

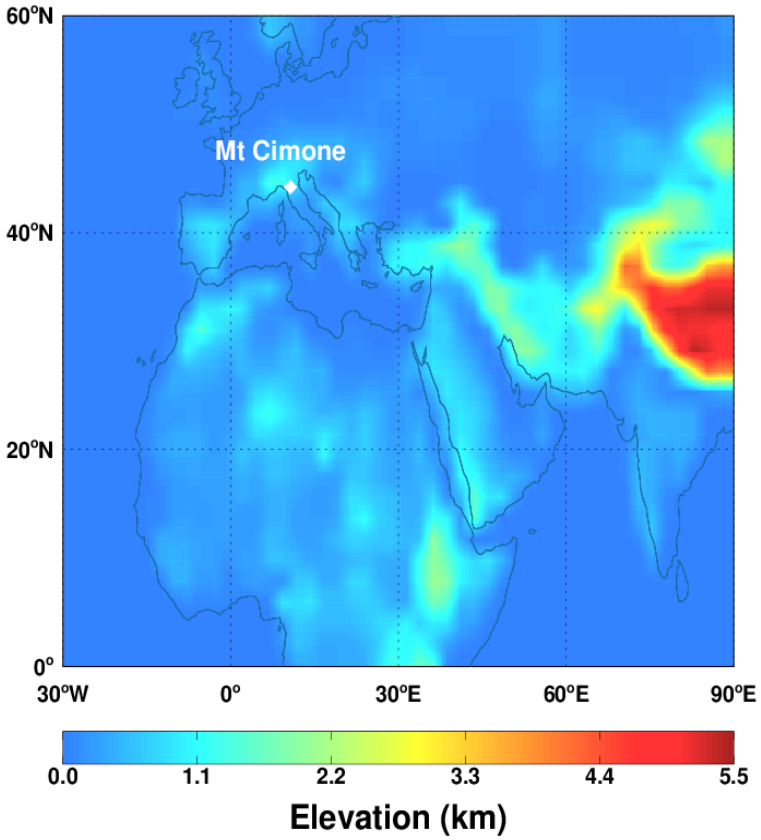

Figure 1. Surface elevations (km) in the model. The white dot indicates the location of Mt. Cimone (44°12' N, 10°42' E, 2165 m asl).

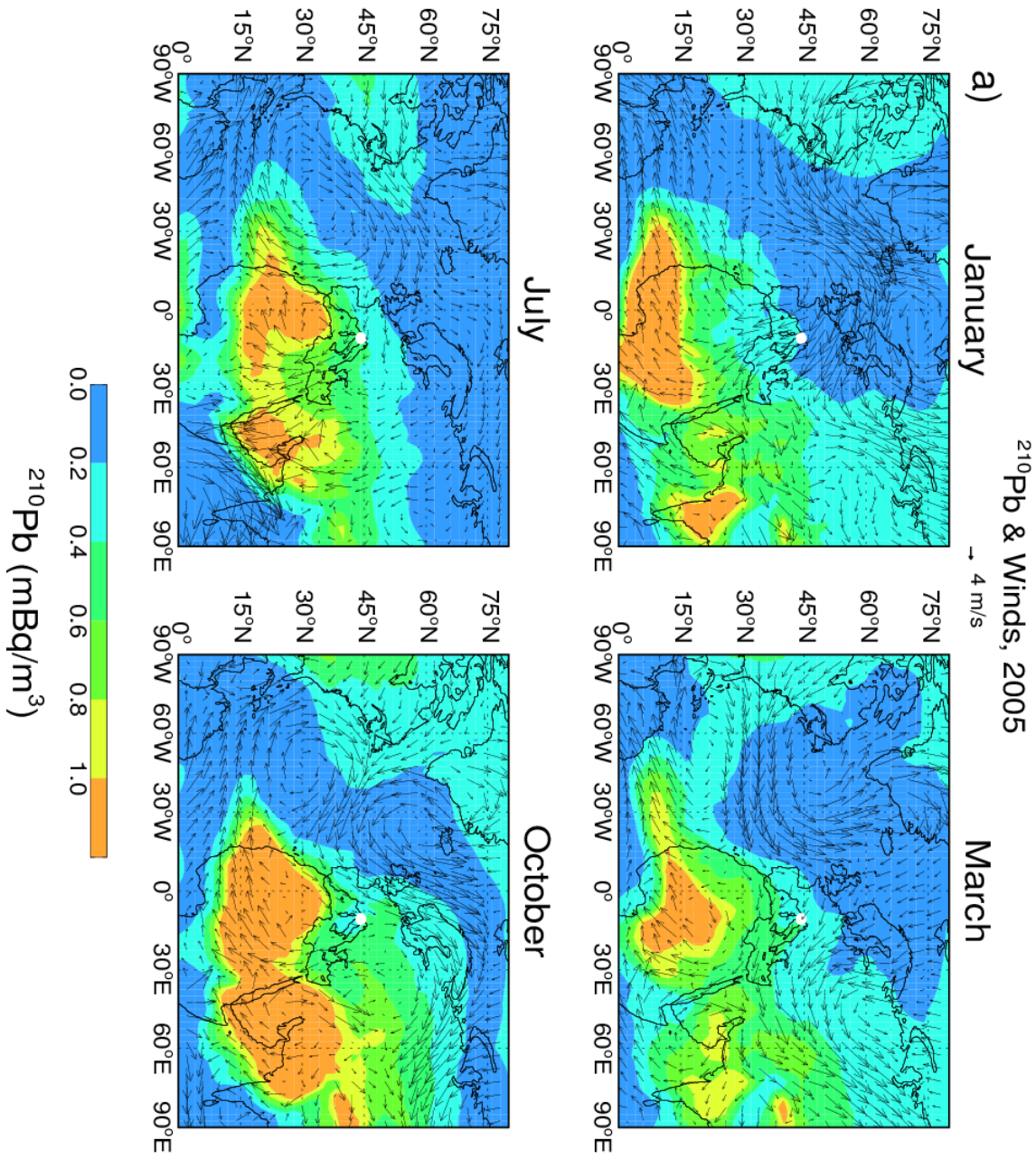

1

2 **Figure 2.** Simulated monthly mean (a) ^{210}Pb concentrations and (b) ^{7}Be concentrations, at the
3 elevation of Mt. Cimone. Arrows represent the seasonality of winds in the MERRA
4 meteorological data. The white dot indicates the location of Mt. Cimone (44°12' N, 10°42' E,
5 2165 m asl). To be continued.

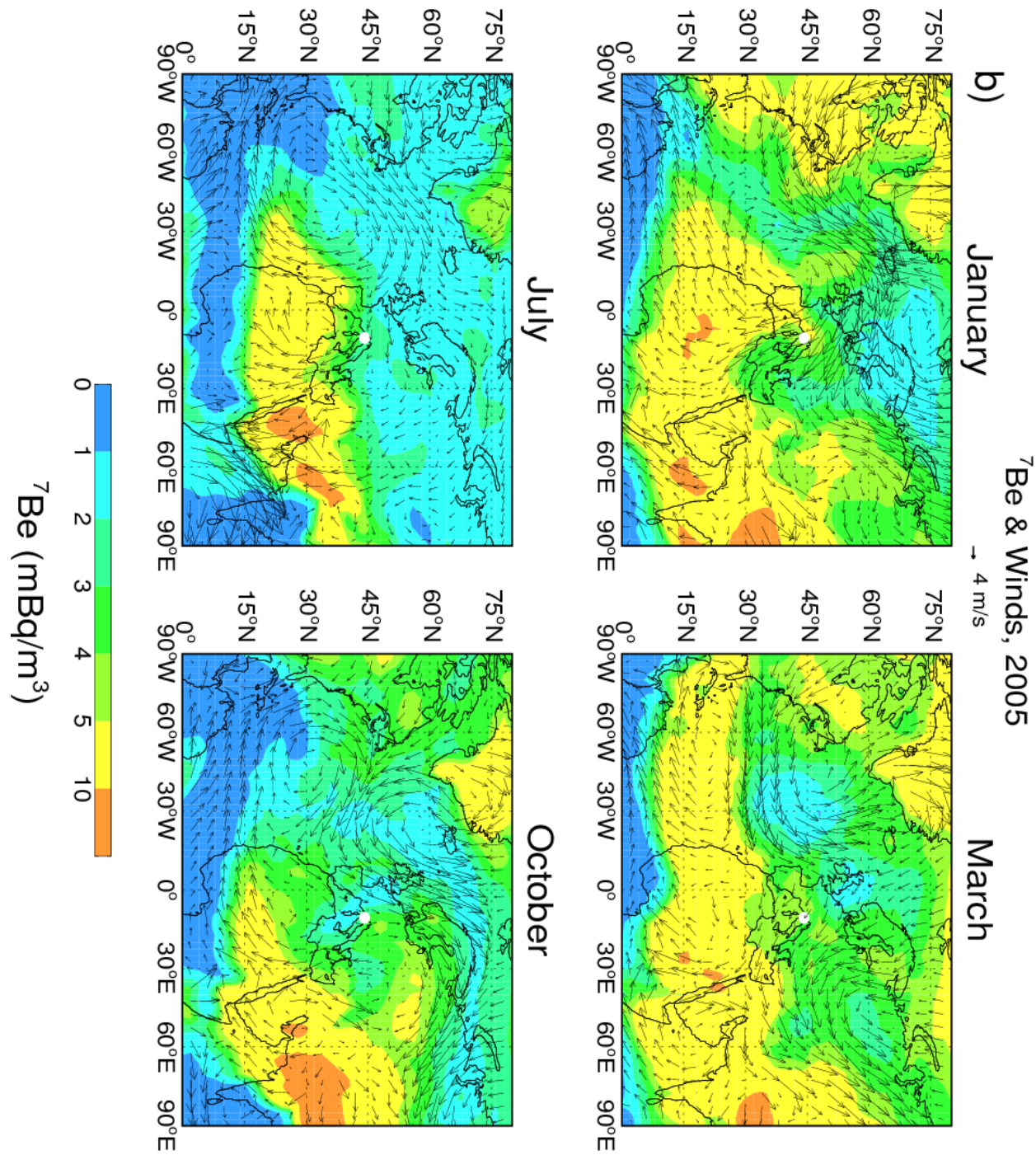

Figure 2. (continued)

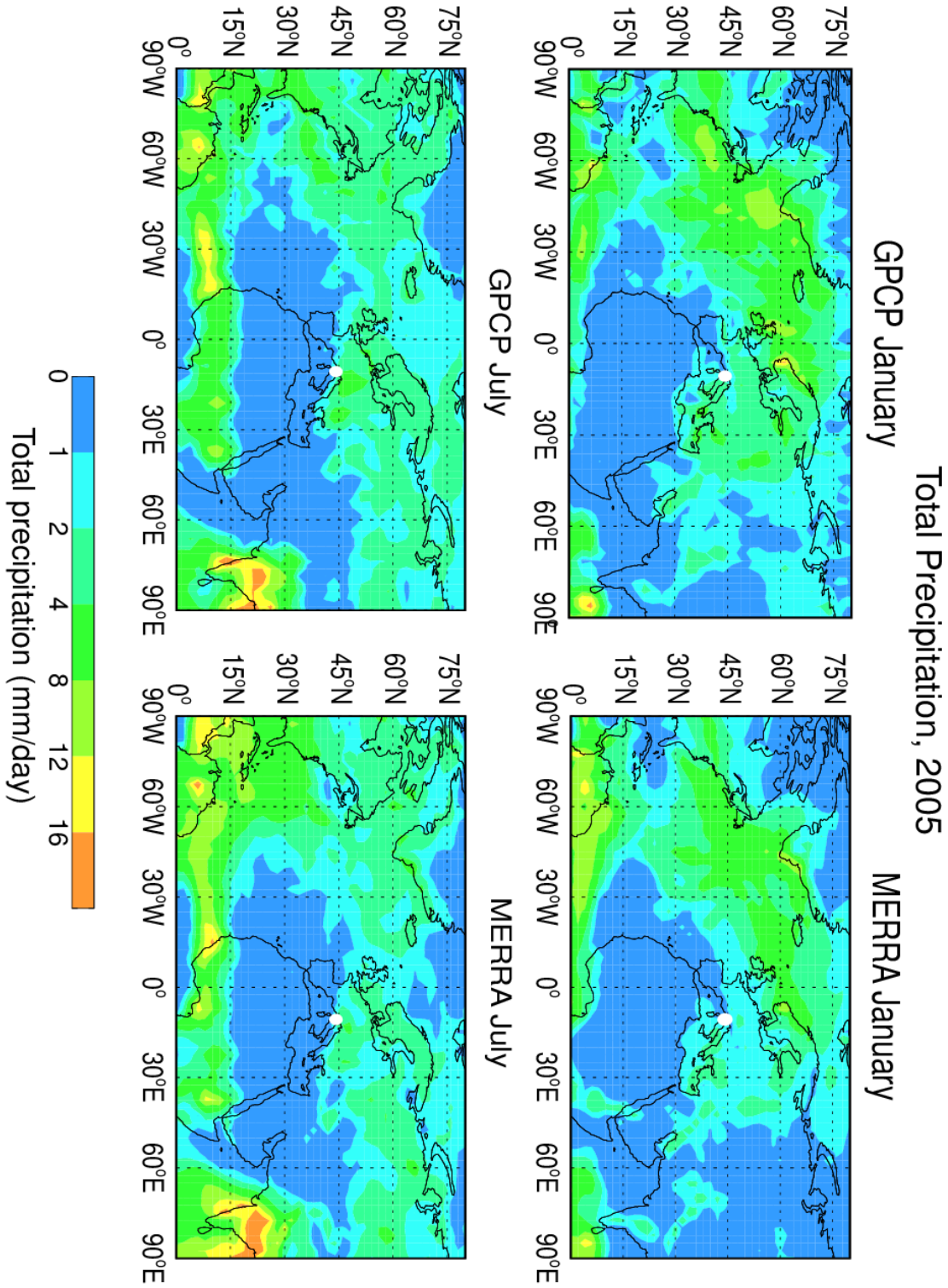

Figure 3. Comparison of the MERRA total precipitation (0-75°N, 90°W-90°E) during January and July 2005 with that in the GPCP observations. The white dot indicates the location of Mt. Cimone (44°12'N, 10°42'E, 2165 m asl).

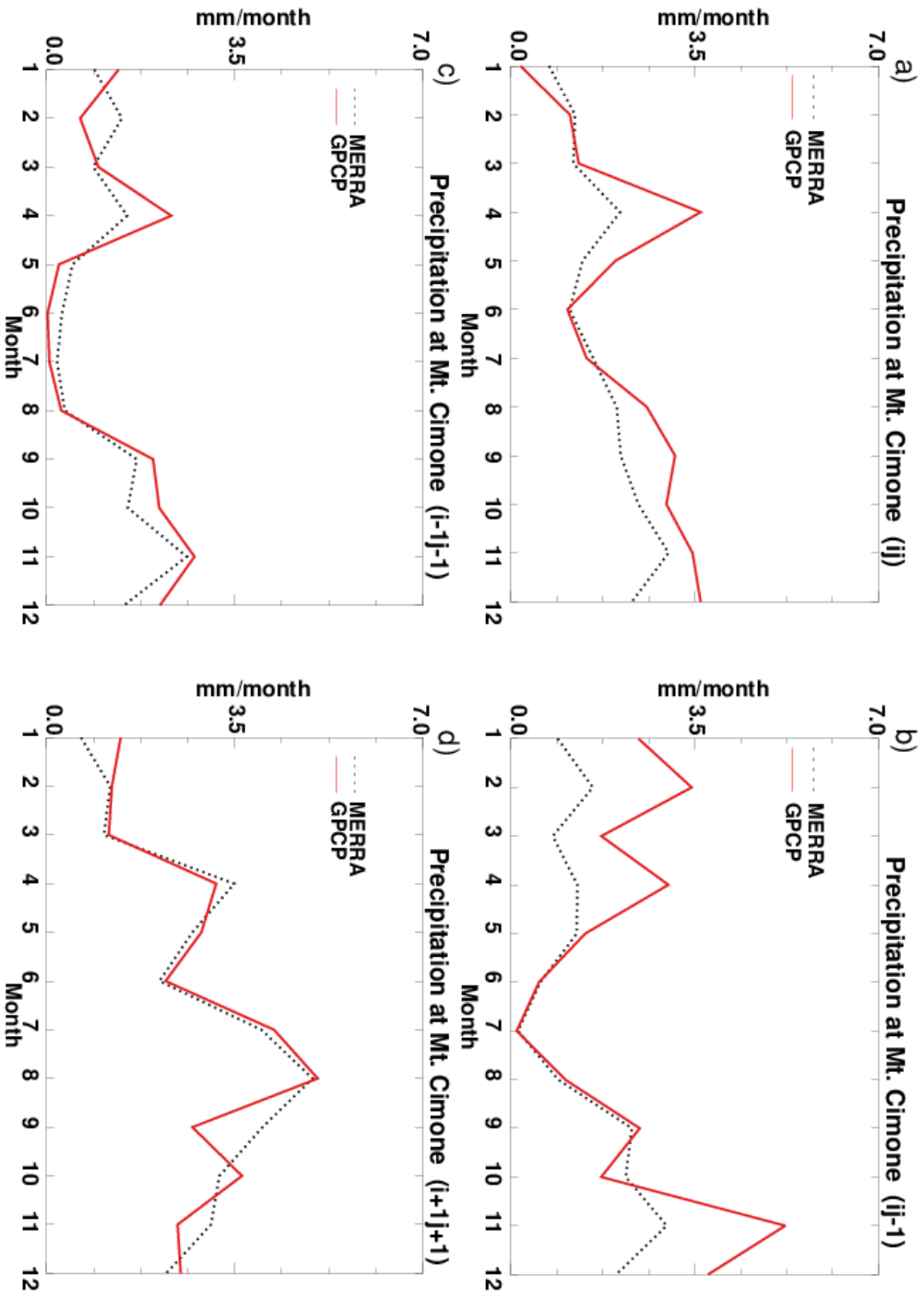

Figure 4. Comparison of the seasonal precipitation at Mt. Cimone in the MERRA meteorological data set with that in the GPCP observations for (a) the model gridbox ("ij") corresponding to the location of Mt. Cimone, (b) the model gridbox ("ij-1") to the west of "ij", (c) the model gridbox ("i-1j-1") to the southwest of "ij", and (d) the model gridbox ("i+1j+1") to the northeast of "ij".

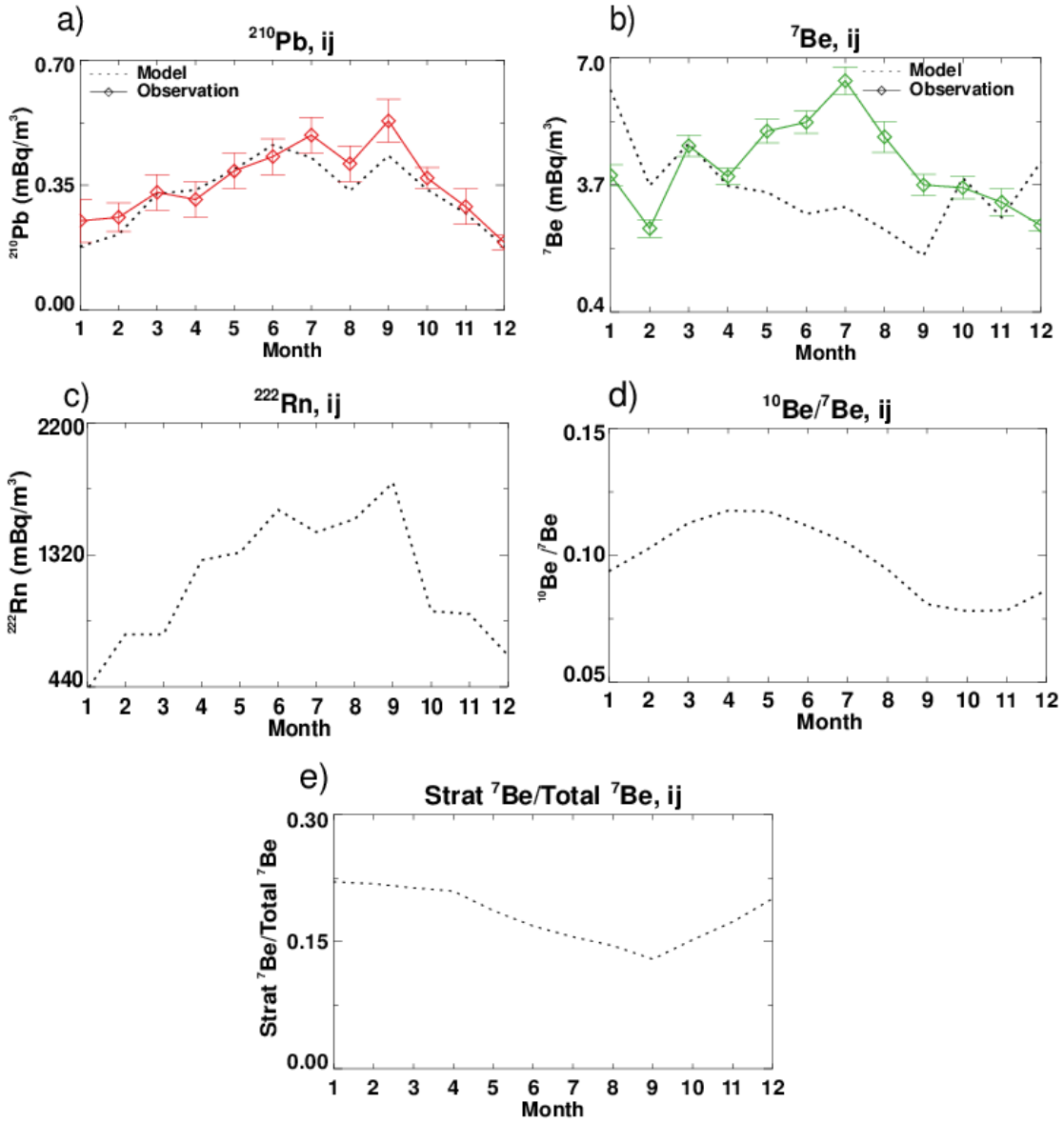

Figure 5 (a,b,c,d,e). Comparison of GMI simulated (black dotted line) monthly (a) ^{210}Pb and (b) ^{7}Be activities with those observed at Mt. Cimone (solid lines) in 2005. Also shown are GMI simulated monthly activities of (c) ^{222}Rn, (d) ^{10}Be/^{7}Be ratios, and (e) strat ^{7}Be/total ^{7}Be ratios. Model values are for the "ij" gridbox corresponding to the location of Mt. Cimone. Vertical bars indicate the uncertainty in observed activities.

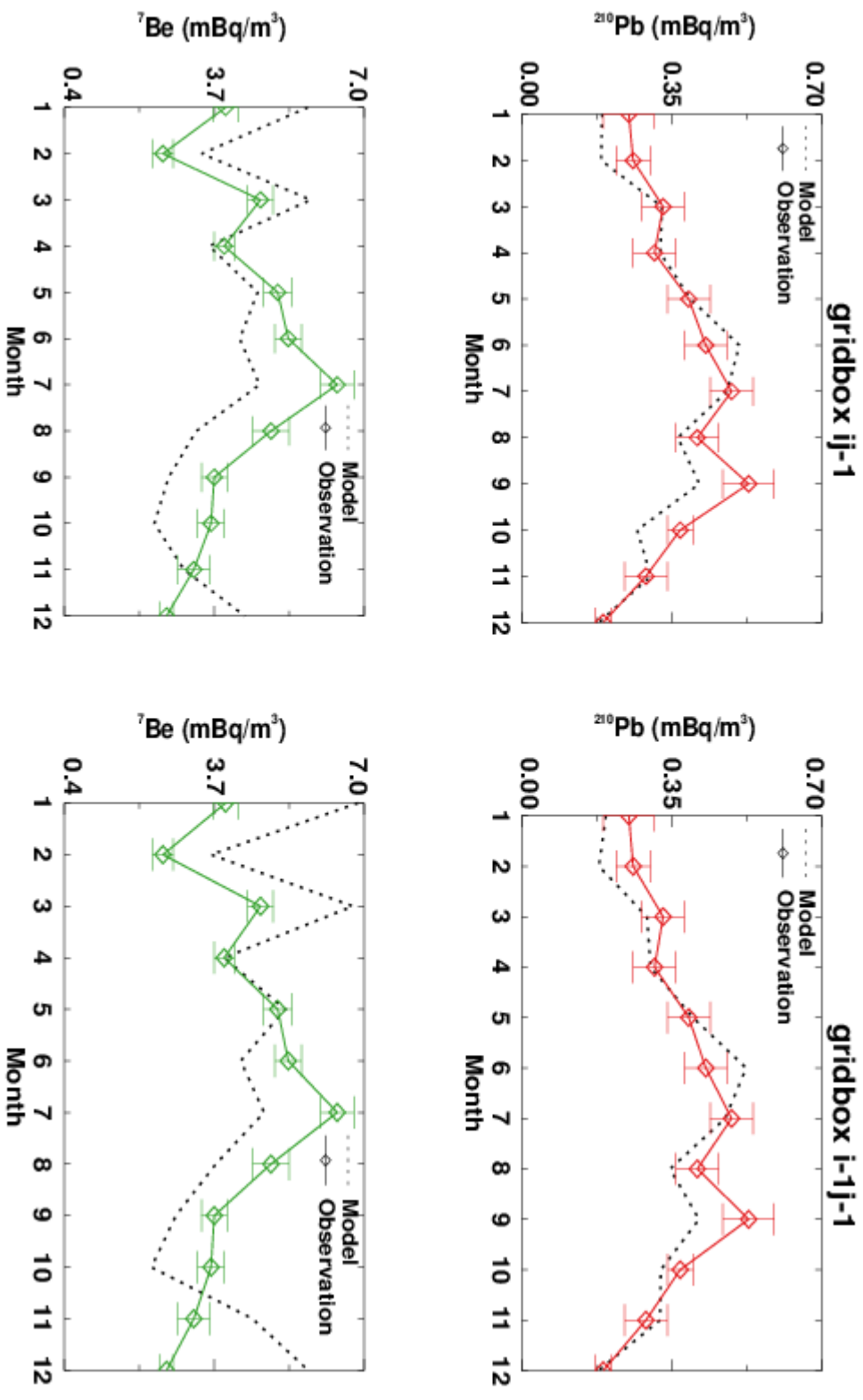

Figure 6. Same as Figure 5(ab), but for the "ij-1" to the south of "ij" (left column) and "i-1j-1" to the southwest of "ij" (right column) grids, respectively.

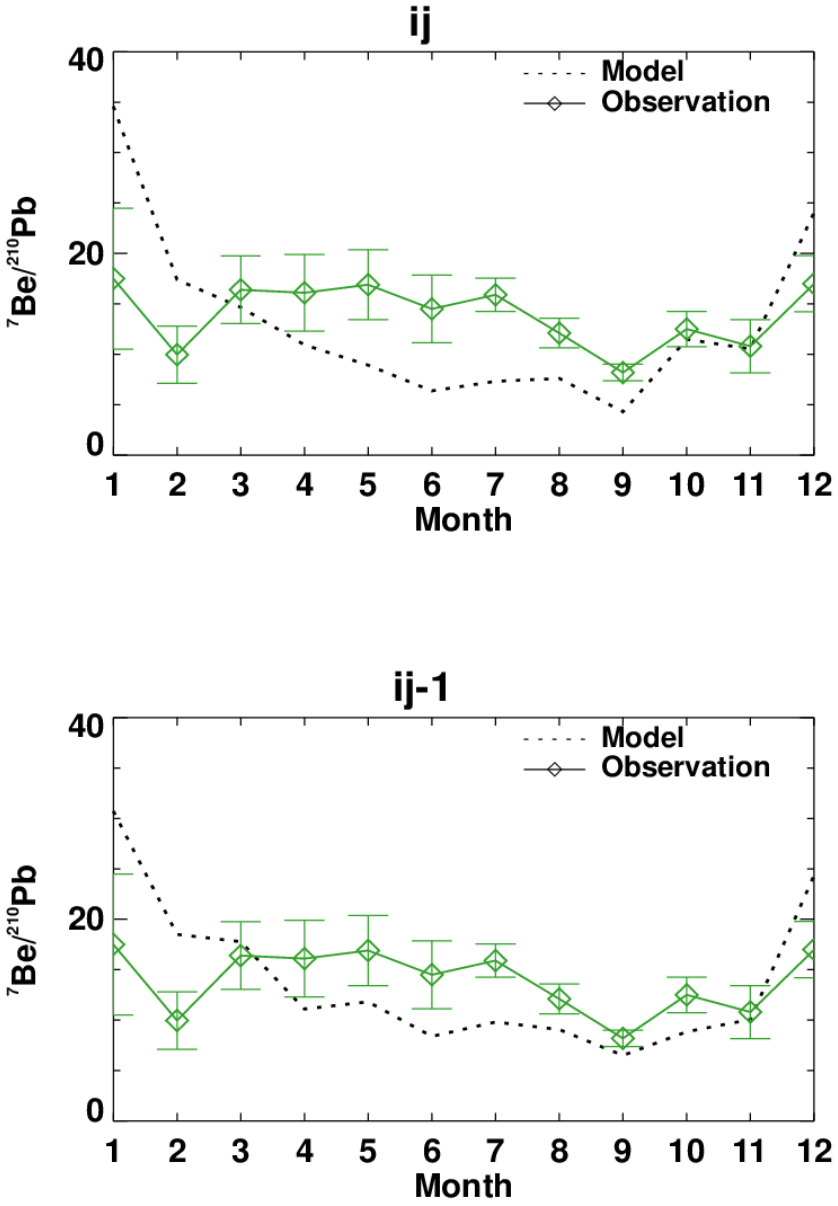

Figure 7. Comparison between GMI simulated monthly $^{7}Be/^{210}Pb$ ratios at the "ij" and "ij-1" grids (black dotted line) and those from the observations at Mt. Cimone (green solid line). Vertical bars indicate the uncertainty in observed activities.

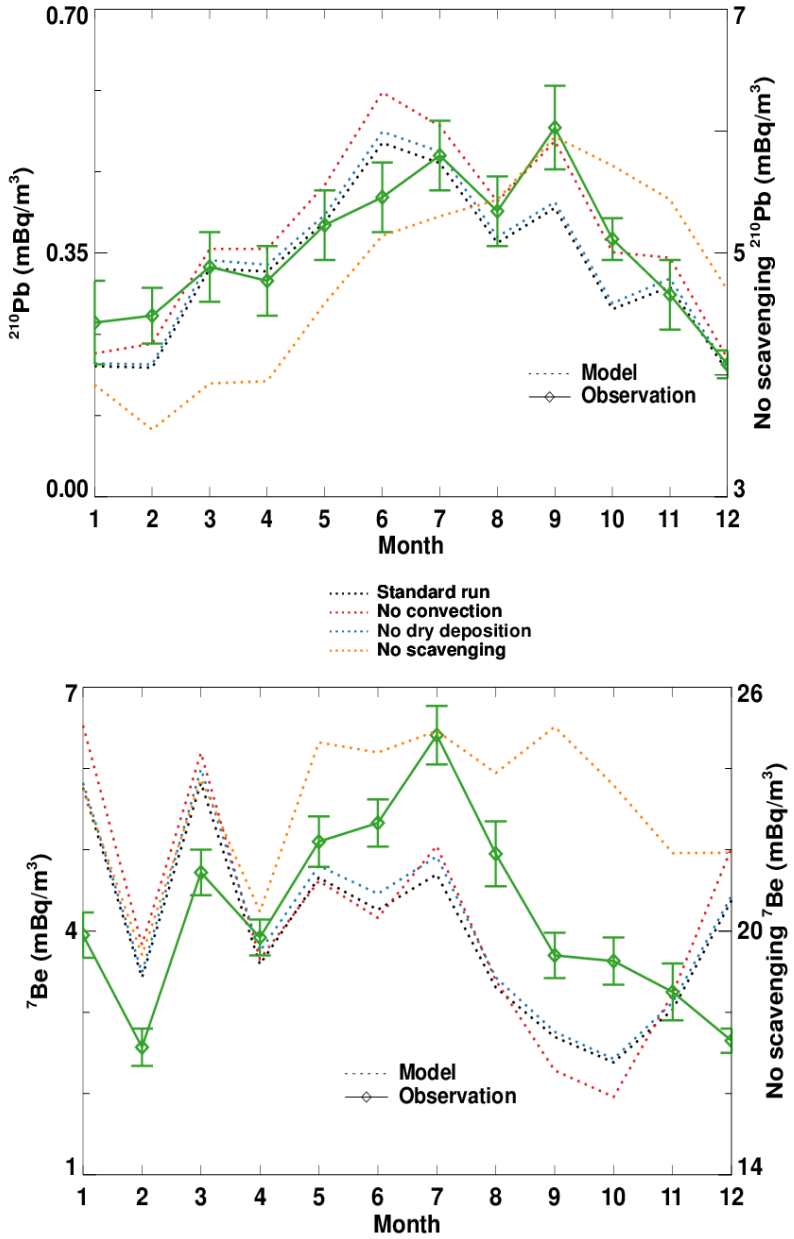

Figure 8. Comparison of GMI simulated monthly ^{210}Pb and ^{7}Be activities at Mt. Cimone between the standard (black dotted line) and the sensitivity runs ("ij-1" grid). The sensitivity runs are those without convective transport/scavenging (red dotted line), without dry deposition (blue dotted line), and without scavenging (orange dotted line; y-axis on the right). The observations are shown as green solid line. Vertical bars indicate the uncertainty in observed activities.

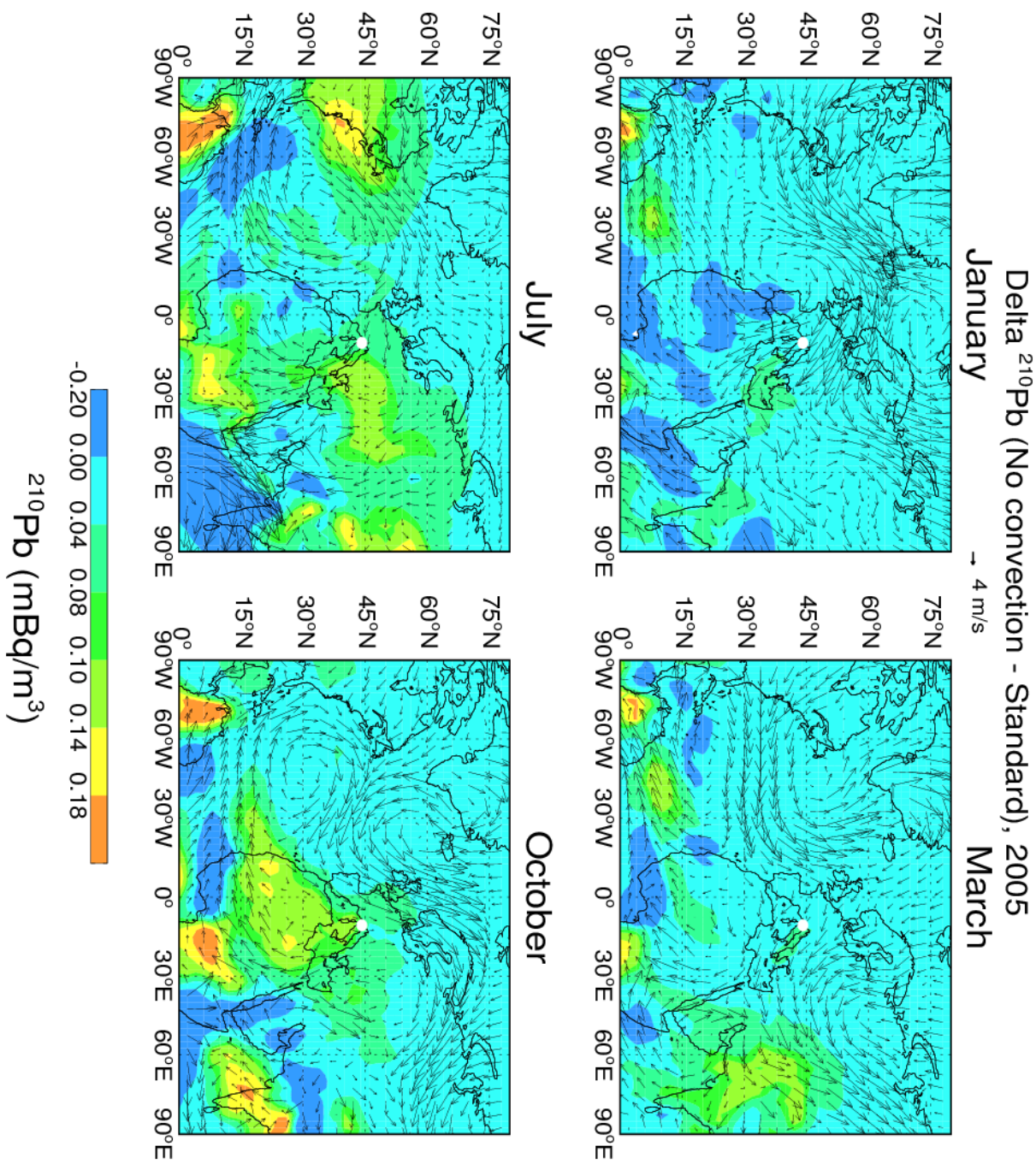

Figure 9. GMI simulated differences of ^{210}Pb concentrations at the elevation of Mt. Cimone between a sensitivity run without convection (i.e., without transport and scavenging in convective updrafts) and the standard run. Arrows denote MERRA winds. The white dot indicates the location of Mt. Cimone (44°12' N, 10°42' E, 2165 m asl).

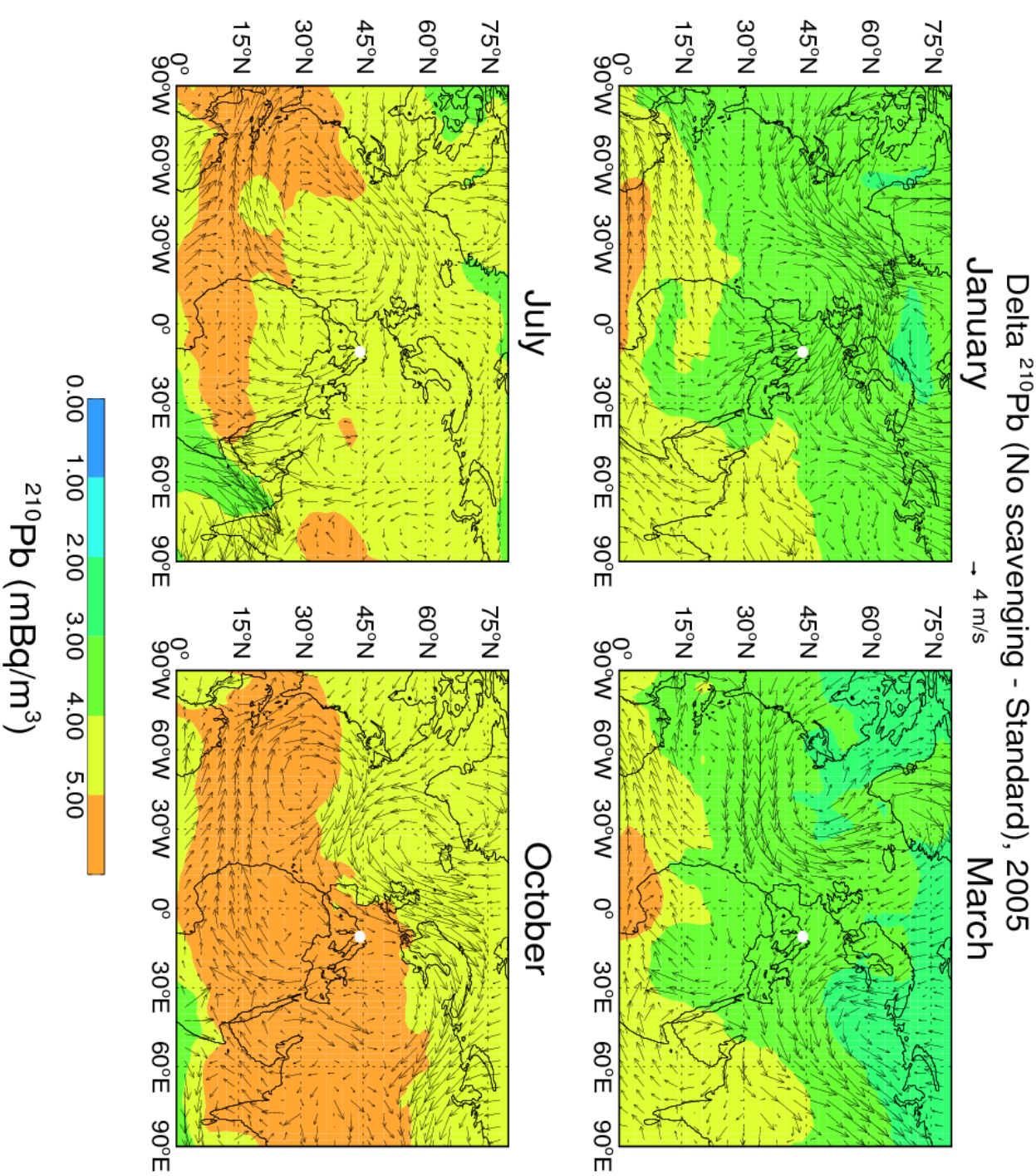

Figure 10. Same as Figure 9, but for a sensitivity simulation where wet scavenging is turned off.

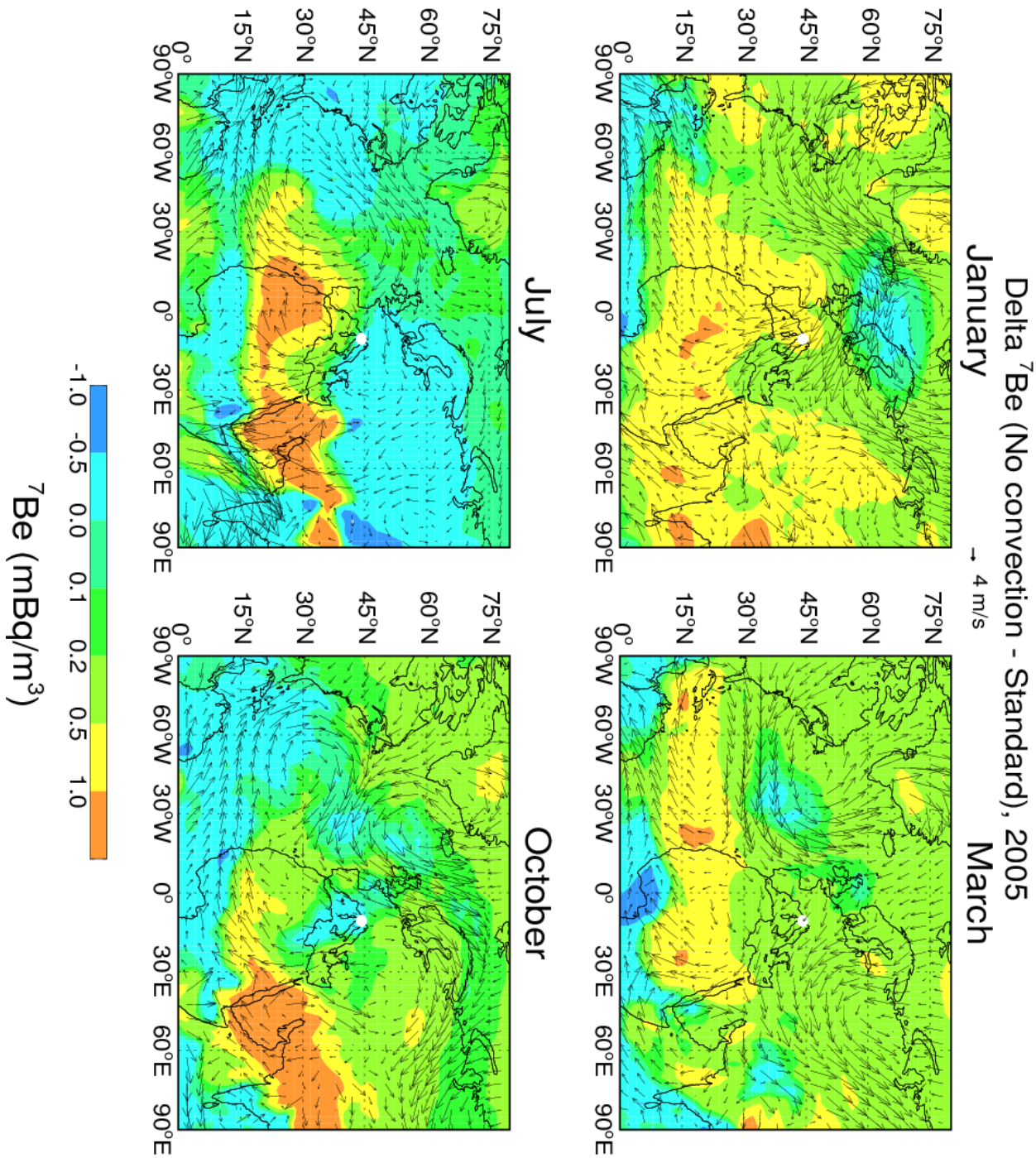

1 **Figure 11.** GMI simulated differences of ^{7}Be concentrations at the elevation of Mt. Cimone
2 between a sensitivity run without convection and the standard run. Arrows denote MERRA
3 winds. The white dot indicates the location of Mt. Cimone (44°12' N, 10°42' E, 2165 m asl).

4

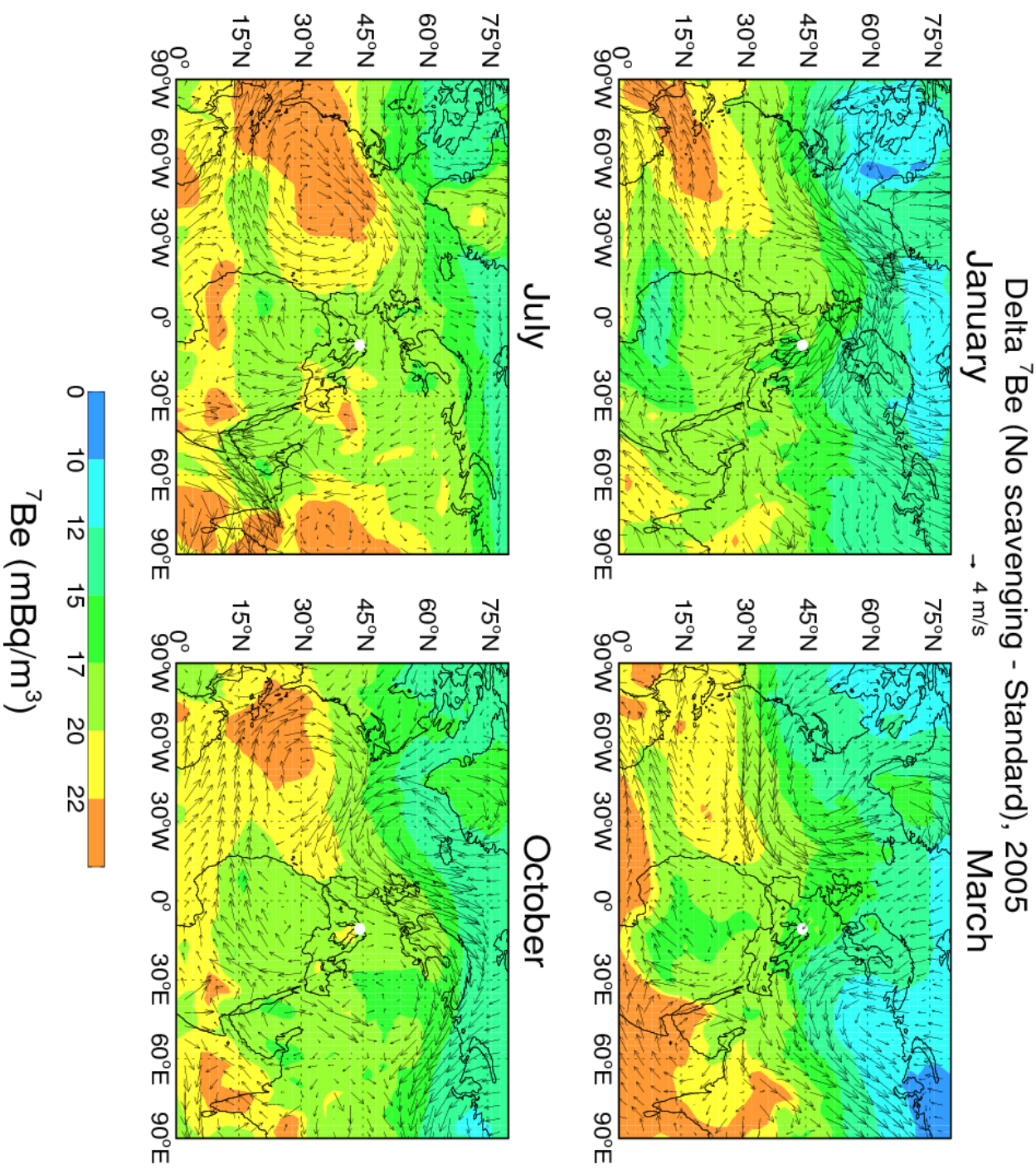

Figure 12. Same as Figure 11 but for the difference between a sensitivity run without wet scavenging and the standard run.

Supplementary Material

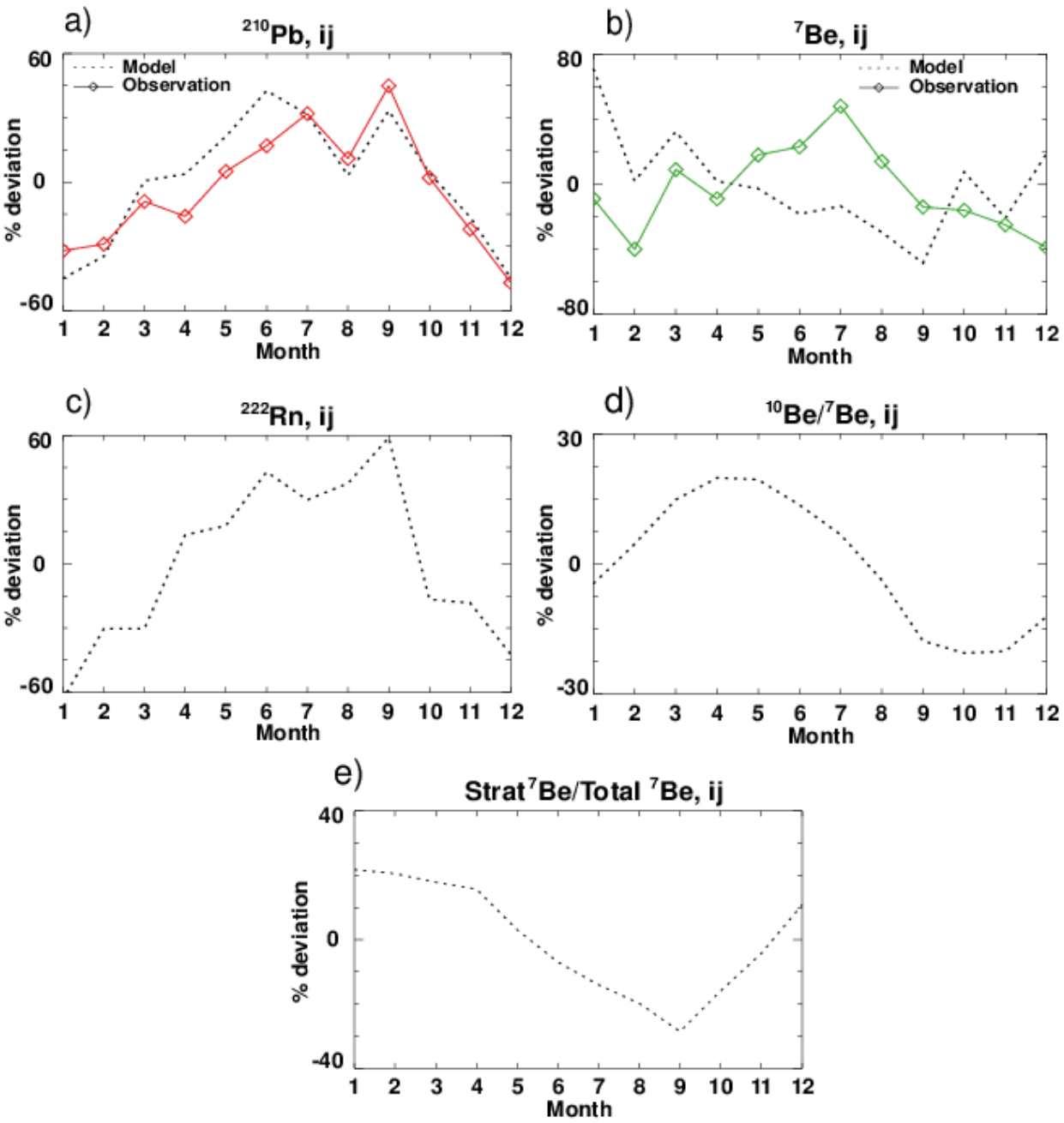

SI Figure 1 (a,b,c,d,e). Comparison of GMI simulated (black dotted line) percentage deviations from the annual means of (a) ^{210}Pb and (b) ^{7}Be concentrations with those observed at Mt. Cimone (solid lines). Model values are for the "ij" gridbox corresponding to the location of Mt. Cimone. Also shown are GMI simulated monthly fluctuations of (c) ^{222}Rn activities, (d) ^{10}Be/^{7}Be ratios and (e) strat ^{7}Be/total ^{7}Be ratios.

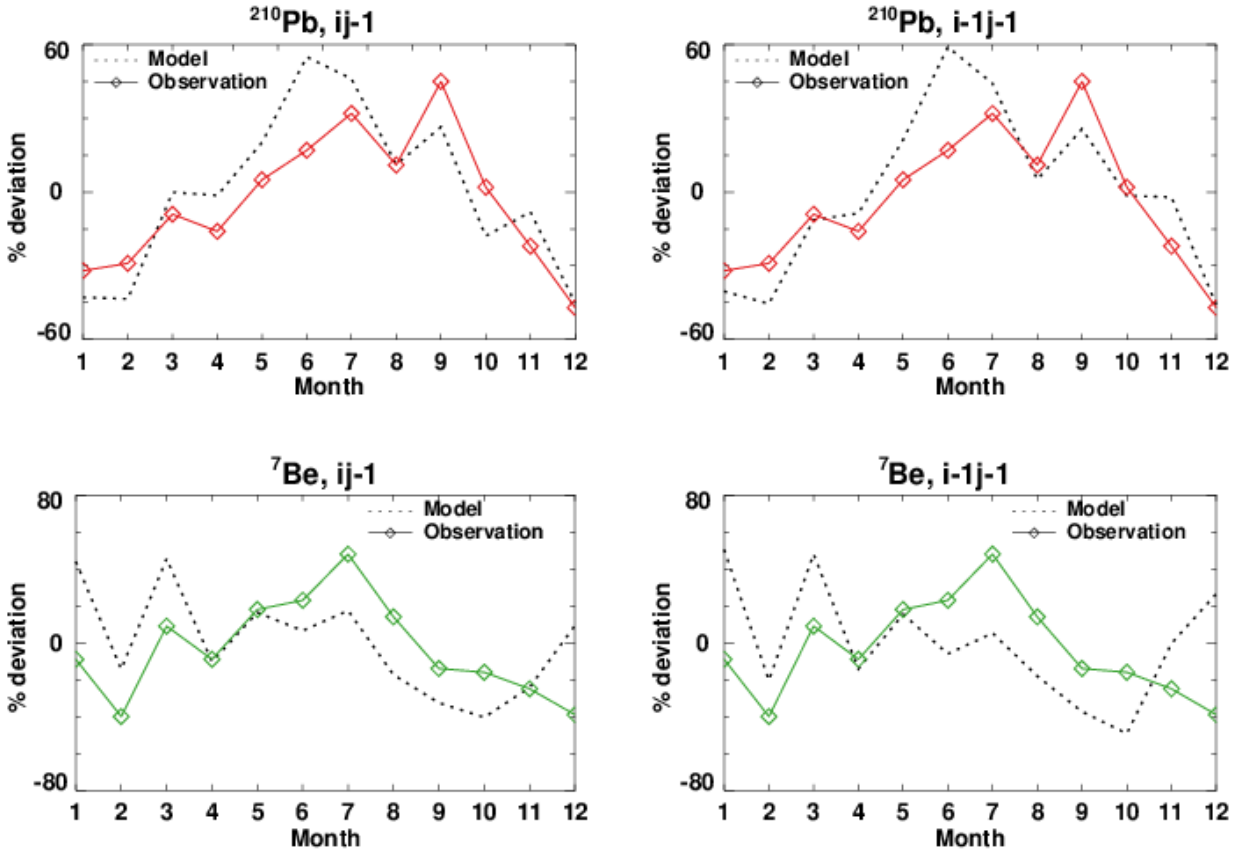

SI Figure 2. Same as SI Figure 1(a, b), but for the "ij-1" grid to the south of Mt. Cimone (left column) and the "i-1j-1" grid to the southwest of Mt. Cimone (right column), respectively.

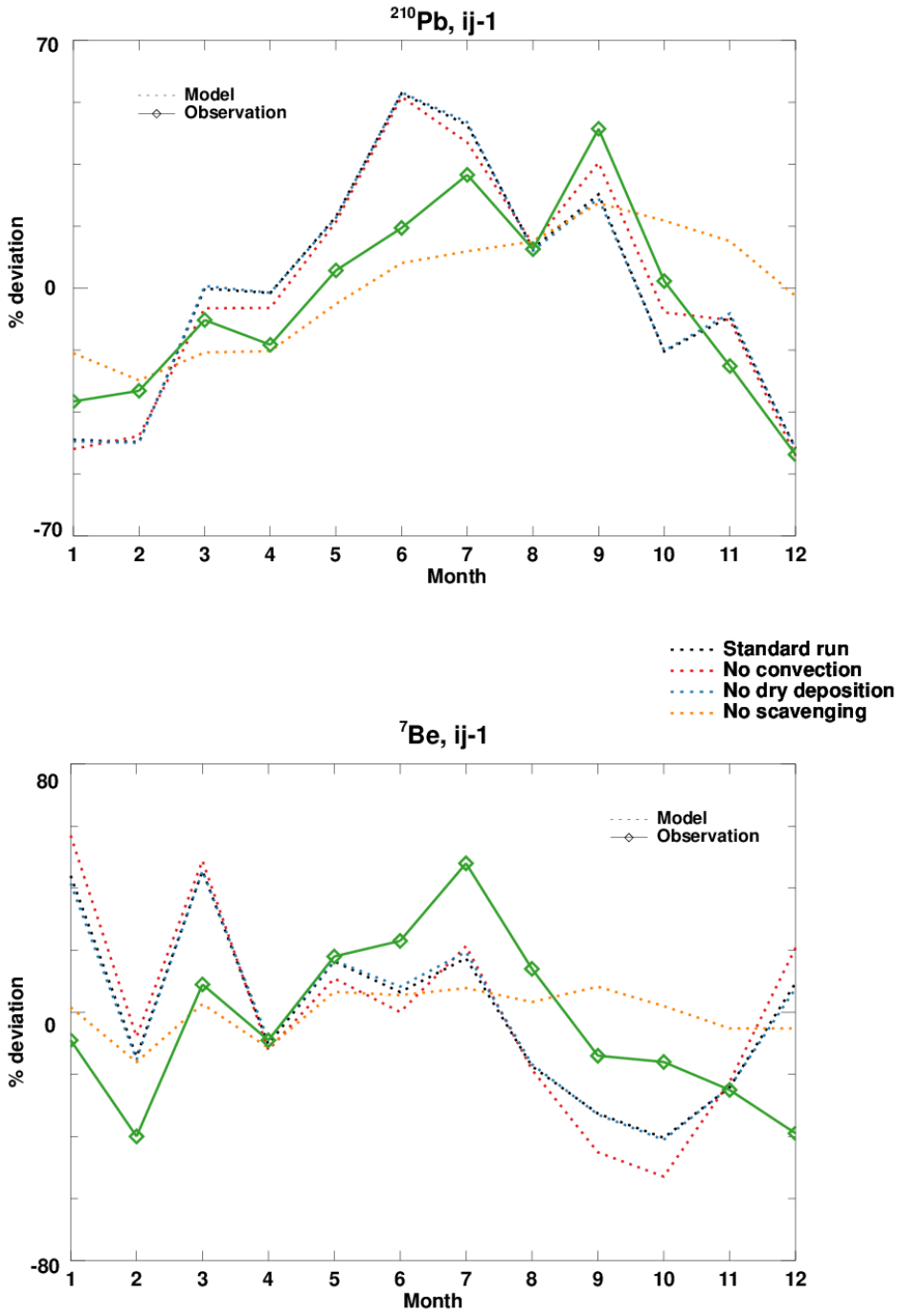

SI Figure 3. Comparison of GMI simulated monthly percentage fluctuations of ^{210}Pb and ^{7}Be at Mt. Cimone ("ij-1" grid) between the standard (black dotted line) and the sensitivity runs. The sensitivity runs are those without convective transport/scavenging (red dotted line), without dry deposition (blue dotted line), and without scavenging (orange dotted line). The observations are shown as green solid line.

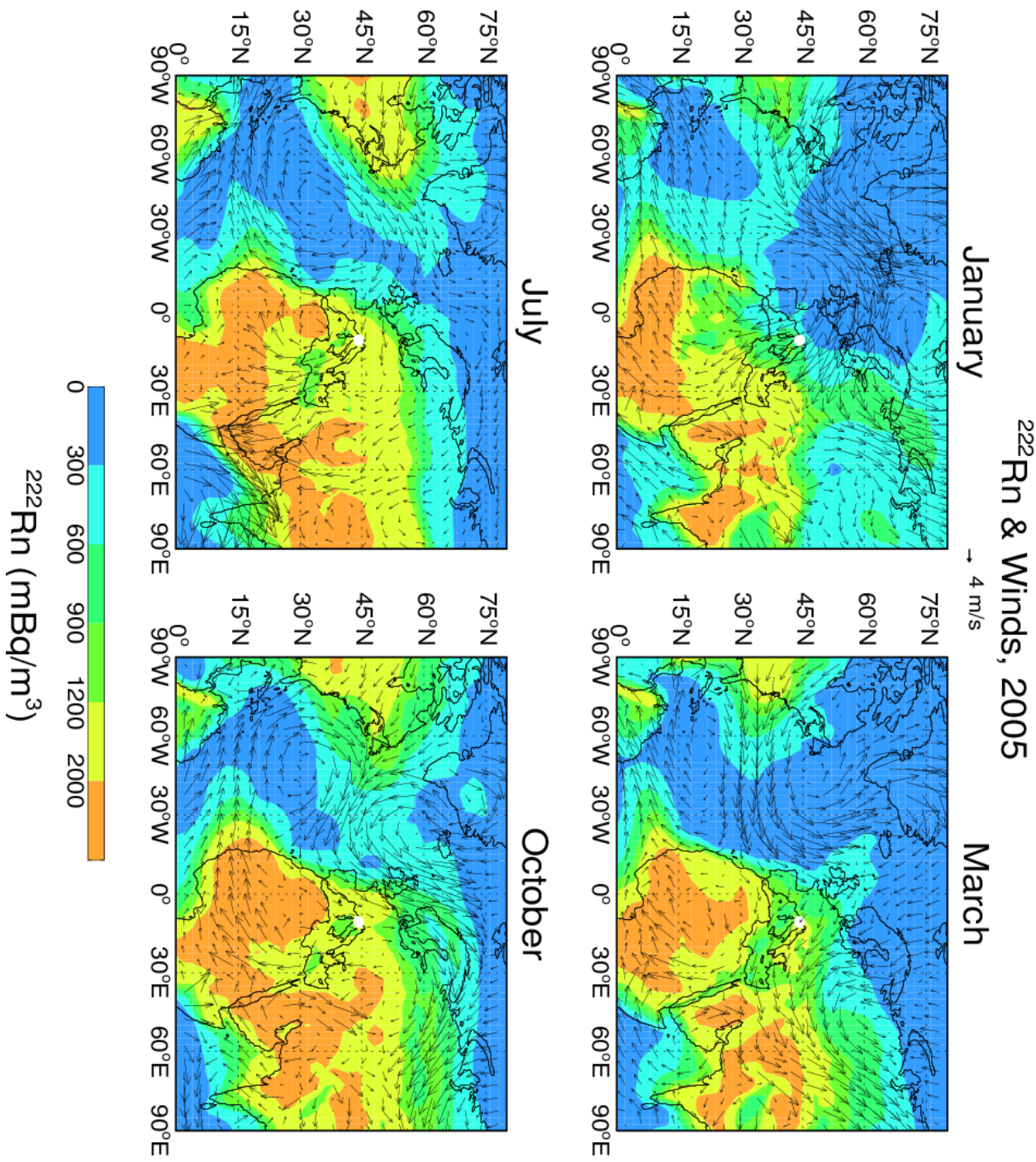

SI Figure 4. Simulated monthly mean ^{222}Rn concentrations, at the elevation of Mt. Cimone. Arrows represent the seasonality of winds in the MERRA meteorological data. The white dot indicates the location of Mt. Cimone (44°12' N, 10°42' E, 2165 m asl).

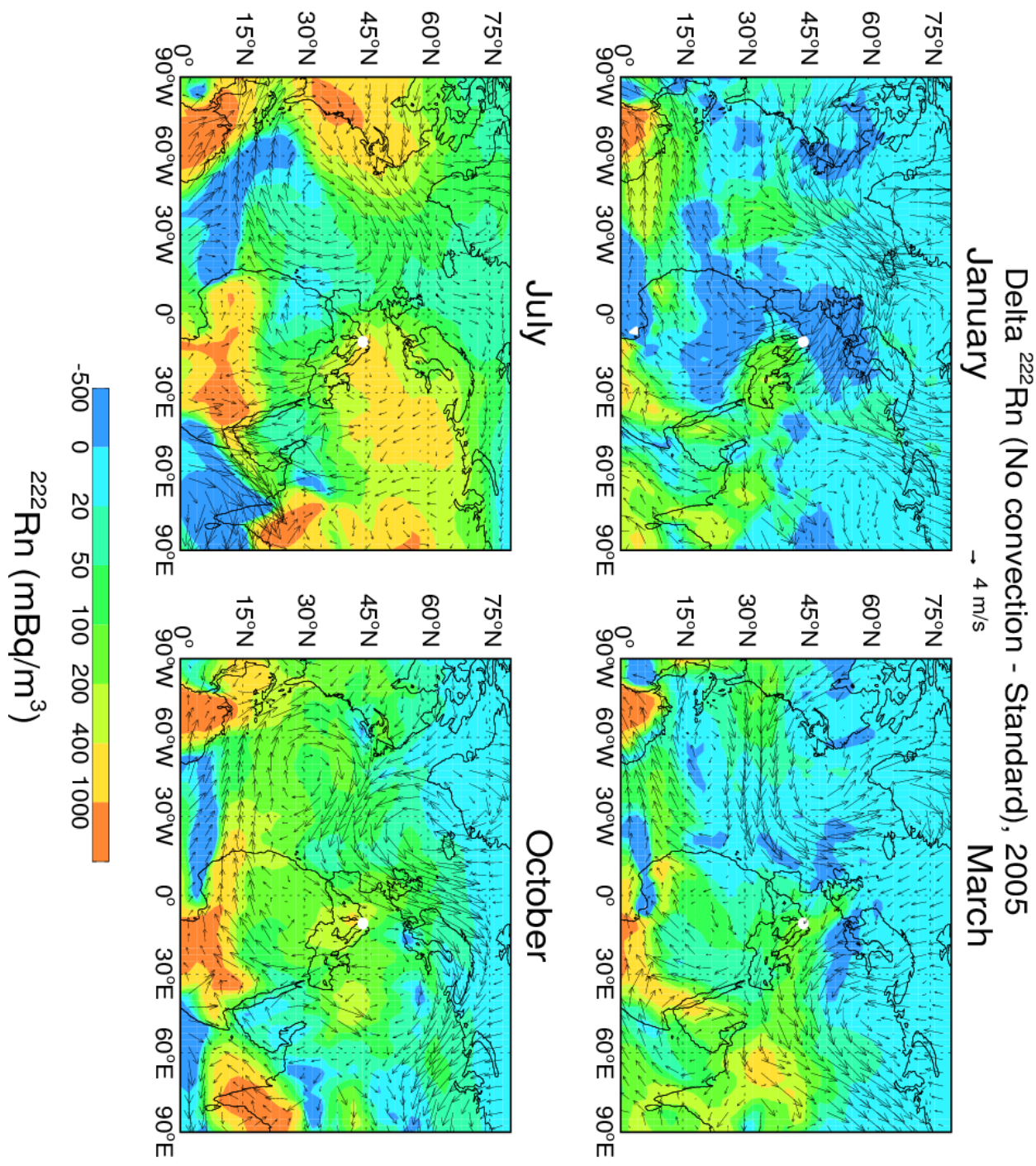

SI Figure 5. GMI simulated differences of ^{222}Rn concentrations at the elevation of Mt. Cimone between a sensitivity run without convection and the standard run. Arrows denote MERRA winds. The white dot indicates the location of Mt. Cimone (44°12' N, 10°42' E, 2165 m asl).